

Customized Mid-Air Gestures for Accessibility: A \$B Recognizer for Multi-Dimensional Biosignal Gestures

Momona Yamagami
momona@rice.edu
Electrical and Computer Engineering,
Rice University, Houston
Houston, Texas, USA

Claire L. Mitchell
The Information School | DUB Group,
University of Washington, Seattle
Seattle, Washington, USA

Alexandra A.
Portnova-Fahreeva
Paul G. Allen School of Computer
Science & Engineering, University of
Washington, Seattle
Seattle, Washington, USA

Junhan Kong
The Information School | DUB Group,
University of Washington, Seattle
Seattle, Washington, USA

Jennifer Mankoff
Paul G. Allen School of Computer
Science & Engineering, University of
Washington, Seattle
Seattle, Washington, USA

Jacob O. Wobbrock
The Information School | DUB Group,
University of Washington, Seattle
Seattle, Washington, USA

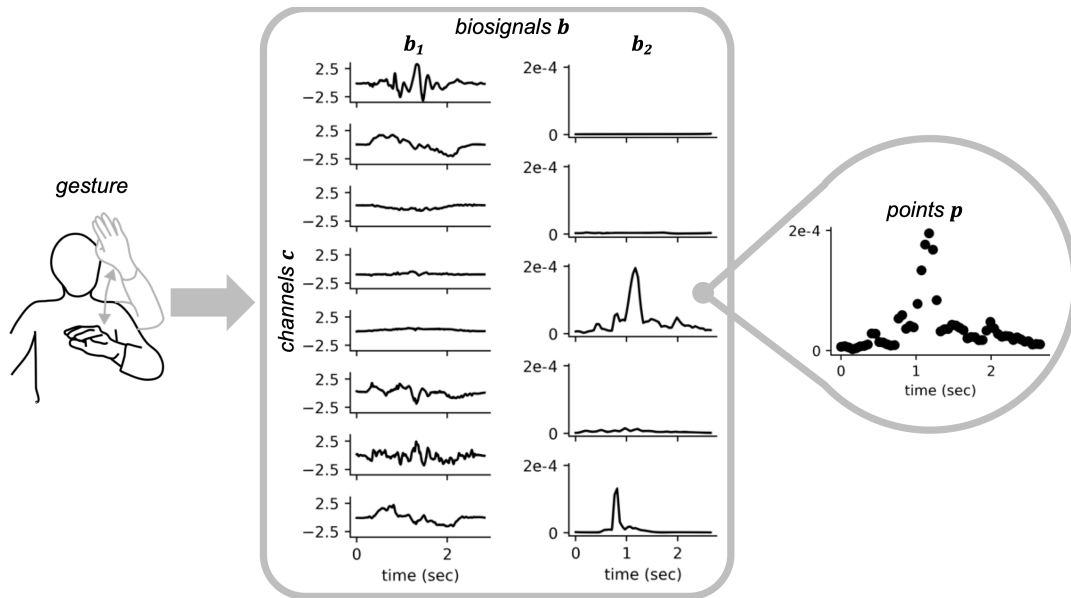


Figure 1: In biosignal interfaces, a user’s gesture, whether a candidate gesture G or a stored template gesture T_i , results in one or more biosignals b . Measured biosignal amplitudes can vary heavily depending on the sensor and measurement method. In this example, the left biosignal (biosignal b_1) amplitudes range from -2.5 to 2.5 , whereas the right biosignal (biosignal b_2) amplitudes range from 0 to 2×10^{-4} . Each biosignal can have one or more biosignal channels c . Each channel contains one-dimensional signals composed of points p .

Abstract

Biosignal interfaces, using sensors in, on, or around the body, promise to enhance wearables interaction and improve device accessibility for people with motor disabilities. However, biosignals are multi-modal, multi-dimensional, and noisy, requiring domain expertise to design input features for gesture classifiers. The \$B-recognizer enables mid-air gesture recognition without needing expertise in biosignals or algorithms. \$B resamples, normalizes, and performs dimensionality reduction to reduce noise and enhance signals relevant to the recognition. We tested \$B on a dataset of 26 participants with and 8 participants without upper-body motor disabilities performing personalized ability-based gestures. For two

Permission to make digital or hard copies of all or part of this work for personal or classroom use is granted without fee provided that copies are not made or distributed for profit or commercial advantage and that copies bear this notice and the full citation on the first page. Copyrights for components of this work owned by others than ACM must be honored. Abstracting with credit is permitted. To copy otherwise, or republish, to post on servers or to redistribute to lists, requires prior specific permission and/or a fee. Request permissions from permissions@acm.org.

Conference acronym 'XX, June 03–05, 2018, Woodstock, NY

© 2018 Association for Computing Machinery.
ACM ISBN 978-1-4503-XXXX-X/18/06... \$15.00
<https://doi.org/XXXXXXXX.XXXXXXX>

conditions (user-dependent, gesture articulation variability), \$B outperformed our comparison algorithms (traditional machine learning with expert features and deep learning), with > 95% recognition rate. For the user-independent condition, \$B and deep learning performed comparably for participants with disabilities. Our biosignal dataset is publicly available online. \$B highlights the potential and feasibility of accessible biosignal interfaces.

CCS Concepts

• **Human-centered computing** → **Gestural input; Empirical studies in accessibility.**

Keywords

datasets, accessibility, gestures, algorithms

ACM Reference Format:

Momona Yamagami, Claire L. Mitchell, Alexandra A. Portnova-Fahreeva, Junhan Kong, Jennifer Mankoff, and Jacob O. Wobbrock. 2018. Customized Mid-Air Gestures for Accessibility: A \$B Recognizer for Multi-Dimensional Biosignal Gestures. In *Woodstock '18: ACM Symposium on Neural Gaze Detection, June 03–05, 2018, Woodstock, NY*. ACM, New York, NY, USA, 20 pages. <https://doi.org/XXXXXXX.XXXXXXX>

1 Introduction

Mid-air gesture interfaces using biosignals measured from sensors in, on, or around the body are becoming more ubiquitous for device interactions, including with wearables [72], virtual and augmented reality [3], and public displays [51]. Biosignal gesture interfaces can improve device accessibility for people with upper-body motor disabilities, as they enable people to interact with various body parts, and—in inclusive interfaces—fully take advantage of their diverse abilities [22, 65, 66, 74, 75]. However, translating biosignals into gesture classifications without domain expertise is challenging because biosignals are multi-modal, multi-dimensional, and noisy. To ensure that emerging biosignal gesture interfaces can be personalized to a specific user's motor abilities, user interface developers need biosignal gesture recognizers that can be integrated easily into prototypes without the need for extensive biosignal or algorithm development knowledge. Almost 20 years ago, Wobbrock *et al.* presented a \$1 unistroke recognizer [69] motivated by making pen gestures easier to recognize in user interface prototypes. Inspired similarly, here we offer \$B, a recognizer for mid-air multi-dimensional biosignal gestures collected from 34 participants, 26 of whom have upper-body motor disabilities.

Traditionally, biosignal gesture recognition has been applied in assistive technologies (e.g., an active prosthesis to replace a limb [37]) and rehabilitation (e.g., an exoskeleton for functional recovery after stroke [27, 58]). In these fields, feature selection by biosignal experts [2, 19, 31] (e.g., number of zero-crossings, maximum signal amplitude) is an important component of gesture recognition and requires domain knowledge of important features of the specific biosignal. More recently, deep learning has been used to automatically derive important features from biosignal data for prosthetics and exoskeleton applications [9, 59]. The need for deep domain expertise makes biosignal gesture recognition challenging, and designing and training neural networks on the large amounts of biosignal data needed for model learning can be prohibitive.

For 2-D stroke-gesture interfaces, such as with pens, fingers, or mouse cursors, the \$-family gesture recognizers [6, 7, 60–62, 69] have had a tremendous impact on supporting lightweight gesture recognition prototyping, being successfully adopted in both research and commercial applications. However, biosignal gesture recognizers, especially those that leverage data from multiple channels and support users with diverse abilities, have unique constraints that make the \$-family gesture recognizers unsuitable. First, biosignals can be noisy due to sensor failure, human movement, and poor contact between the user and biosensor. This can make it challenging to scale and rotate the dataset, as even minor fluctuations in the gesture due to noise can have significant impact in the scaling and orientation of the biosignal gesture. Second, not all channels are equally important in biosignal interfaces. For example, if a biosensor collects data from both the right and left hand, but an individual only performs a movement with their right hand, the data collected from the left hand contains no meaningful information to classify the gesture. Similarly, biosignals are often highly redundant due to the redundancy in human motor control and contain similar movement information within multiple channels. Third, different biosignals can be measured on vastly different scales, including the measurement amplitude and sampling frequency. All of the aforementioned issues make the \$-family gesture recognizers unsuitable for biosignal gesture recognition.

In this work, we designed \$B, a new biosignal gesture recognizer for mid-air gestures. In contrast to recent state-of-the-art biosignal recognizers that utilize sophisticated learning techniques [16, 52, 72] or biosignal-specific features [2, 19, 31], \$B is simple and uses known techniques like resampling, normalization, and principal component analysis. Like the popular \$1 recognizer [69] before it, this simplicity makes \$B easily approachable to non-experts, and has the potential to enable accessible and customized gesture recognition for next-generation prototypes, including for virtual and augmented reality, gaming, and wearables applications. For example, consider a college student who is developing an accessible virtual reality game using kinematic input obtained from video data. Without \$B, the student may have to investigate and implement kinematics features or replicate state-of-the-art algorithms like [52], a significant endeavor. Or, the student can implement \$B, run short tests to choose two parameters (number of time points, principal components), and continue development.

We tested \$B on mid-air gestures collected from 34 participants, 26 of whom had upper-body motor disabilities. Overall, \$B outperformed our comparison algorithms—1) a support vector machine applied to expert features (traditional ML) and 2) a multi-layer convolutional and long-short term neural network on normalized data (deep learning)—when the models were personalized to each user. Specifically, \$B had a recognition error rate of 9% ($SD=9$), whereas traditional ML had 18% ($SD=13$) and deep learning had 17% ($SD = 14$). When the same gestures were articulated at a different time, faster, or larger than originally performed, \$B continued to outperform traditional ML and deep learning, with recognition error rates of 24% ($SD=31$), 62% ($SD=32$), and 44% ($SD=29$), respectively. Lastly, although \$B did not perform as well as deep learning for user-independent models overall (recognition error rate of 29% ($SD=19$) vs. 22% ($SD=17$), respectively), the two algorithms performed similarly for participants with disabilities (recognition error

rate of 34% ($SD=23$) vs. 30% ($SD=18$), respectively). Thus, as with prior \$-family recognizers, \$B is a simpler, more straightforward approach to recognizing gestures that yield better or similar performance as more complex, expert methods.

In this work, we offer the following research contributions [67]:

- *Artifact.* The introduction of \$B, an algorithm inspired by the prior \$-family recognizers that takes into account the unique challenges associated with multi-dimensional biosignal gestures.
- *Study.* Evaluation of \$B for 26 participants with and 8 participants without upper-body motor disabilities, demonstrating a low recognition error rate (9%, $SD=9$) compared to traditional ML (18%, $SD=13$) and deep learning (17%, $SD=14$) algorithms for gestures personalized to a user’s motor abilities. The \$B recognizer is robust against variations in how a gesture is articulated and performs comparably when tested across participants with disabilities.
- *Dataset.* A released dataset of 26 participants with and 8 participant without upper-body motor disabilities performing different gestures that are personalized to their abilities, when the same gestures are performed analogously, and when the same standardized gestures are performed across different participants.

Our work improves the ability to incorporate biosignal gestures into user interfaces for new and emerging technologies without the need for domain expertise, including for people with upper-body motor disabilities.

2 Related Work

Our work builds on prior research on gesture customization in HCI, both using biosignal interfaces as well as more commonly used interfaces such as touchscreens [69]. The prior work demonstrates that currently available biosignal interfaces in HCI are not accessible for people with upper-body motor disabilities. Further, we discuss prior research on body-machine interfaces for health and rehabilitation, which many of the biosignal HCI applications build on. While body-machine interfaces provide a starting point for biosignal interfaces for HCI applications, direct translation of body-machine interface approaches to HCI are challenging and require novel adaptations for translation to HCI applications [21].

2.1 Gesture Customization in HCI

Gesture customization is important for improving device accessibility [74], accounting for cultural differences [70], and improving memorability of the gesture meaning compared to standardized gestures [44]. In recent years, gesture recognition and customization for mid-air gesture input have received increasing academic attention [16, 29, 40, 50, 52, 72]. Many focus on wrist-worn IMU sensors which record linear acceleration and rotational velocity in three-dimensions [40, 52, 72]. Other work focuses on non-invasive neural interfaces like electromyography (EMG) [16, 29, 50], which measure muscle electrical activity. Preliminary work with biosignal interfaces takes inspiration from research in prosthetics to use expert-derived features [50] or distance metrics [29] to classify gestures. These works highlight the potential of using biosignal interfaces for HCI applications.

More recent works leverage large datasets (500+ [72] to 5000+ [16] participants) to develop deep learning models that are shared among the end-users. For work that supports gesture customization, one- or

few-shot learning (an approach that leverages a pre-trained model to extend to unseen samples [64]), has been used to enable gesture customization from few samples [52, 72]. While these algorithms can achieve up to 97% accuracy even with only one template gesture [52], there are several limitations with these approaches. First, the algorithms are complex to train and integrate into a project for developers not well-versed in algorithm development and deep learning. Second, the algorithms require large datasets [16, 72] or applying novel transformations to the dataset [52], which requires additional expertise. Third, such gesture customization methods rely on pre-trained models that use demonstrations from people without motor disabilities, which may not extend well to people with upper-body motor disabilities. Our work aims to fill this gap and make mid-air gesture customization accessible for user interface developers, who may not have access to expertise in algorithm development or large datasets.

In HCI, the \$-family recognizers for touch-based gestures has received wide acclaim in both academic and industry settings [6, 7, 60–62, 69]. The \$-family focuses on algorithms that are easy to implement, contain minimal code, and require only a small number of templates to customize gestures. Towards this goal, the \$-family recognizers focus on transforming gestures by scaling and rotating and then comparing distances between candidate and template gestures for gesture recognition. Crucially, the algorithms are simple to implement, requiring little expertise in gesture recognition and can identify gestures with only a few templates. This work is the first in the \$-family to extend these principles to mid-air biosignal interfaces. As emphasized in our introduction and algorithm section, biosignal interfaces pose unique challenges compared to touchscreen gestures that require new innovations in transforming and comparing the candidate and template gestures.

2.2 (In)Accessible Biosignal Input in HCI

Despite the proliferation of devices that use biosignals and upper-body movements for interactions in recent years (e.g., Apple AssistiveTouch [8], hand tracking on Meta Oculus [39]), these interactions remain inaccessible for people with upper-body motor disabilities due to the lack of gesture customization [38, 43] and assumptions underlying these gesture interfaces [74]. People with motor disabilities experience challenges like difficulty with performing the motion precisely, fatigue, and not being able to do the desired motion at all due to their disability [38, 74].

Much of the research on improving accessibility to biosignal interfaces have been formative, focusing on understanding the accessibility limitations of existing devices [38], characterizing the effect of upper-body motor disability on biosignal input [63], or defining new gestures for device interaction [22, 74, 75]. For example, Vatavu and Ungurean [63] investigated the accessibility of stroke and motion gestures on wearable devices worn on the wrist, finger, and head, finding that participants with disabilities find motion-gestures performed in mid-air much easier than stroke-gestures performed on wearable touchscreens. Carrington et al. [13, 14] explored and developed a set of input devices (“chairables”) designed specifically for individuals who use wheelchairs. Other work investigated people’s preferences on input modality [36] or defined above-the-neck [75], eyelid [22], and upper-body [74] gesture

sets that are inclusive of people with upper-body motor disabilities. While these formative studies are critical to understanding the needs and challenges of individuals with motor disabilities, they fall short of addressing the challenge that there are no algorithms designed for non-expert developers that support accessible and customizable biosignal gesture recognition in HCI.

2.3 Body-Machine Interfaces for Health and Rehabilitation

While biosignal interfaces have only recently started to be investigated in HCI [21], these signals have been extensively studied and implemented for body machine interfaces (BoMIs) in health and rehabilitation applications [2, 9, 19, 27, 31, 37, 58, 59]. For example, inertial measurement units (IMU) and electromyography (EMG) sensors can be used to detect motion intention for lower-limb stroke rehabilitation [58]. Similarly, EMG has been used extensively for active prosthesis control to replace lost limbs [37].

To perform gesture recognition for BoMI applications, windowed gesture data (e.g., 200 ms of data) are continuously classified, usually by extracting expert-derived features such as the number of zero-crossing or maximum signal amplitude [2, 19, 31]. Which expert features to extract depends on the biosignal type and application, and there is no one universal set of expert features. More recently, deep learning has been successfully used in BoMI applications for gesture recognition [9, 37] and continuous control [10]. Deep learning can be used to learn nonlinear relationships between the expert features and the gesture recognition [37] or to extract features directly from the biosignal data in a data-driven manner [9, 72].

Despite these advances, direct translation of the techniques developed in this field to HCI applications is difficult for several reasons [21]. First, research in BoMIs predominantly focuses on uninterrupted and continuous gesture recognition because the BoMI is being constantly used throughout the day. Therefore, in health and rehabilitation applications, biosignal gestures are usually continuously recognized (e.g., classify biosignals every 200 ms), rather than the complete gesture being classified (e.g., detect when a gesture begins and ends, and then recognize the entire gesture trajectory). In HCI applications, however, device interactions are often intermittent, which requires new approaches for biosignal gesture recognition [21]. Additionally, BoMI researchers and practitioners are experts in biosignal interfaces, with domain expertise of appropriate features and algorithms for their biosignal and task. Our work aims to support user interface prototypes and developers who do not have this domain expertise so that they can still incorporate biosignal gesture recognition into their HCI prototypes.

3 The \$B Recognizer

In this section, we present an overview of \$B, a “biosignal gesture recognizer.” We describe the components of this recognizer and detail how the unique properties of biosignals were considered during development of the recognizer. A pseudocode of the algorithm can be found in Appendix A.

3.1 Considerations for a Biosignal Recognizer

In mid-air biosignal recognition, gestures are multi-dimensional signals sampled over time, resulting in high-dimensional signals. These high-dimensional signals, if used in \$-family recognizers [6, 7, 60–62, 69] or other conventional HCI gesture recognition algorithms

(e.g., [49]) without further processing or an understanding of the biosignal type, could result in misrecognized gestures due to the data being manipulated without considerations for the unique challenges of biosignal gestures.

First, biosignals may be measured on different scales. If multiple biosignals are being used to characterize and recognize the gesture, the inherent characteristics of the different sensors must be considered. First, some types of sensors may have a higher sampling frequency than others, leading to an unequal sample number for a given gesture. This can be resolved with resampling over time. Second, measurement amplitudes for different biosignals may be orders of magnitude apart from one another. For example, EMG data is usually measured in volts, with signal amplitudes around 10^{-4} volts, whereas accelerometer data is usually measured in terms of the gravitational constant, g (where $1g = 9.81m/s^2$), with amplitudes around 1 to $10g$. Without proper resampling and scaling, it would be difficult to compare different biosignals (Fig. 1, Fig. 4). To normalize the amplitudes, one can employ a calibration scheme where users are asked to flex their muscles as hard as they can [73] or move their arms in a random pattern [48]. However, this adds additional burden on the user to perform calibration and is not desirable in a user interface.

Second, biosignals can be extremely noisy, and even channels that contain important information may be corrupted (Fig. 2, dark and light blue lines). Sensor failure, human movement, or poor connection between the sensor and the human are all potential sources of noise [17, 18]. Additionally, some biosignals such as electromyography (EMG) signals, which quantify muscle electrical activity, can be highly stochastic and motor disabilities could cause unintended large signal amplitudes causing outliers. This can make it challenging to adopt simple scaling methods, as is done in previous \$-family recognizers [6, 7, 60–62, 69].

Third, in biosignal interfaces, not all channels are equally important (Fig. 2, black dotted line). In the simplest example, consider a biosensor that captures movement from both arms, but the user only moves their left arm to perform a gesture. The biosignal data collected from the right arm contains no useful information to recognize the gesture. Therefore, simply adapting the amplitude of the points to fit a bounding box may not be beneficial if the entire biosignal channel is solely noise. Similarly, biosignal interfaces can be highly redundant and contain similar information within multiple channels (Fig. 2, dark and light blue lines). Consider the scenario where a biosensor that captures movement information is placed on the wrist and the forearm. If the individual is moving their entire arm to perform a gesture, the two sensors contain redundant information about the movement. While redundant information is not necessarily an issue for gesture recognition, noise in multiple redundant channels can make it challenging to accurately compare template gestures with the candidate gesture.

To alleviate the large number of channels and noise associated with biosignal data, dimensionality reduction methods that reduce the biosignal channels to a lower-dimensional *latent space* must be employed. However, when performing this transformation, it is important to ensure that gestures from the same gesture class are close in the latent space, so they can be correctly recognized as the same gesture. This is because, depending on how the dimensionality reduction method is applied, noise inherent in biosignal data may

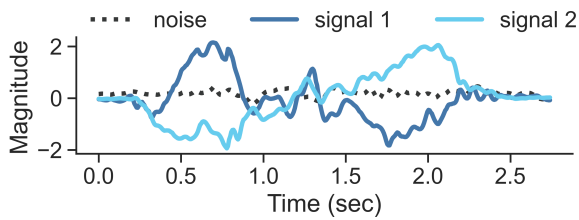


Figure 2: Biosignals can have relevant (signals 1 and 2 in dark and light solid blue) or irrelevant (noise in dotted black) channels for recognition. Both relevant and irrelevant biosignals contain noise that must be reduced to improve recognition accuracy. Additionally, biosignals are often correlated. For example, signals 1 and 2 contain similar information in opposite orientations. As signal 1 increases in magnitude, signal 2 decreases in magnitude and vice versa. Decreasing signal correlations through dimensionality reduction reduces noise and improves recognition accuracy.

affect the transformation and make it challenging to recognize similar gestures in the latent space.

Therefore, in addition to the design criteria originally laid out for the \$1 recognizer [69], the \$B recognizer must:

- (1) Scale biosignal data without the need for user calibration while maintaining differences in signal amplitude between relevant and irrelevant channels and ignoring biosignal measurement outliers;
- (2) Decrease biosignal noise and redundancy prior to gesture recognition;
- (3) Employ dimensionality reduction methods that transform high-dimensional biosignal gestures to a lower-dimensional *latent space* such that gestures from the same gesture class are close to each other in the latent space.

With these design needs in mind, \$B performs biosignal gesture recognition in four steps corresponding to the pseudocode in Appendix A.

3.2 The \$B Algorithm

An unprocessed candidate gesture G or template T_i is made of c channels, which span time, t (Fig. 1). Each channel, depending on its signal origin type, is of biosignal type b_j . The \$B recognizer resamples, translates, normalizes, and decomposes the c channels of the candidate gesture G or template T_i . Candidate gestures G and templates T_i are treated the same for Steps 1 and 2, with both steps being applied when the template points are initially read or when the gesture is performed.

3.2.1 Step 1: Resample Each Time Channel. Biosignal gestures are often sampled at different rates depending on the sensor and data collection software (Fig. 3). Therefore, each biosignal channel must be resampled in time to compare across different biosignals. Additionally, movement speed will affect the number of points in a gesture. To make template gestures and candidate gestures directly comparable even with multiple biosignal inputs or different movement speeds, we first resample each biosignal channel such that all channels have the same number of points. The number of points n to resample each channel to is a parameter that must be explored and defined by the prototyper based on the biosignal of interest.

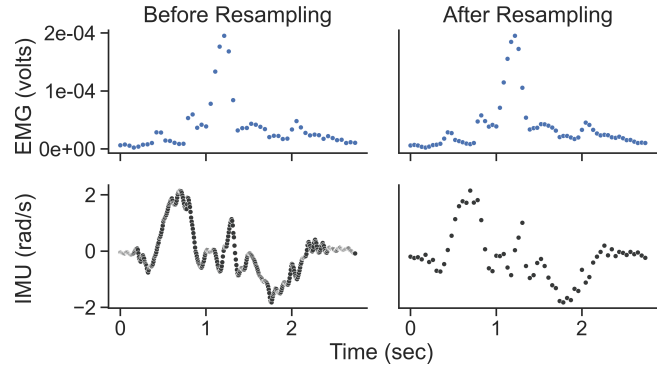


Figure 3: Two different biosignals—(top, EMG) electromyography, measures muscle electrical activity; (bottom, IMU) inertial measurement unit, measures linear acceleration and rotation velocity—may have different sampling rates (left), and must be resampled (right) before comparisons are made. Note the two different measurement scales for the EMG signal (around 10^{-4} volts) and the IMU signal (around 2 g).

As biosignal data is usually collected at a set frequency and therefore the points are equally spaced over time, we resample using piecewise linear interpolation. New points are linearly interpolated from the original biosignal amplitude of the two adjacent time points. Depending on whether n is larger or smaller than the number of points measured for a gesture, each channel is either upsampled or downsampled. The first and last point of the new points are equal to the first and last point of the original points. At the end of this step, all channels of all biosignals will have n points.

3.2.2 Step 2: Normalize. After resampling, the gesture is normalized such that each channel has a mean of 0 and a given biosignal across all channels has a standard deviation of 1 (Fig. 4) [30]. This step is important because different biosignals are measured at different magnitudes and can have different means (Fig. 1). This step differs from traditional machine learning normalization methods. Traditionally, each feature (in this case, each biosignal channel) is normalized such that the standard deviation of each channel is equal to one. In the context of biosignal interfaces, this could result in noisy channels (Fig. 4 dotted lines) being overly large in magnitude compared to channels containing relevant signals (Fig. 4 solid lines), which will negatively affect the recognition accuracy as the noise inherent in biosignal interfaces will be inflated. Rather, in \$B, all channels representing a given biosignal are normalized such that the standard deviation for the vector representing all concatenated channels is equal to one. This ensures that after normalization, channels relevant to the recognition are the same order of magnitude across different biosignals and channels irrelevant to the recognition remain small (Fig. 4, right). Normalizing each biosignal across all channels ensures that distance comparisons across different biosignals are within the same order of magnitude.

Normalization to a standard deviation of 1 was chosen over other methods of normalization (e.g., scale such that the maximum amplitude of the biosignal across all channels is equal to 1) because amplitude spikes due to noise can be a concern with biosignals [18]. To ensure that large outliers do not significantly affect the overall

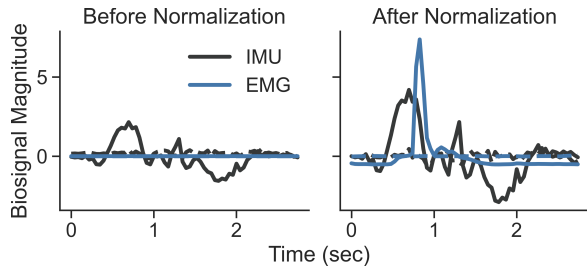


Figure 4: EMG (blue lines) and IMU (black lines) signals before (left) and after (right) normalization. The solid line represents relevant channels for recognition. The dotted line represents irrelevant noise channels. Before normalization (left), the EMG signal and noise are both significantly smaller in amplitude than the IMU signal and noise. After normalization (right), the EMG signal is now on the same scale as the IMU signal. Both EMG and IMU noise channels remain small in magnitude.

distribution of the data, we decided to scale the biosignals such that the standard deviation of each biosignal across all channels is equal to 1. This additionally ensures that relative scaling between relevant and irrelevant channels for a given biosignal is maintained and channels containing noise are not artificially inflated in amplitude.

3.2.3 Step 3: Compute Template PCA. In this step, only template T_i principal components and transformed points are computed and saved after the templates' points are read in, resampled, and normalized. The template principal components will be used to transform the candidate points before recognition in Step 4.

Principal component analysis (PCA) is a dimensionality reduction method that transforms high-dimensional data into a low-dimensional *latent space* [24]. PCA reorients high-dimensional data such that the data's variance (i.e., how much a signal fluctuates from its mean) is maximally explained using only a few major components. It can be a useful tool to extract biosignals relevant to recognition, which usually has a high variance, and remove noise, which usually has a low variance (Fig. 2). It is also a useful tool to decrease correlations and redundant information within a dataset. For this step, we compute the principal components of the template T_i and apply the transformation to the templates' points. Note that the prior normalization step also served as an important preprocessing step for PCA.

To compute the principal components, all biosignals b and channels c must first be vertically concatenated. This results in a data matrix D with c rows and n columns, where c represents the total number of channels across all measured biosignal types and n represents the number of resampled time points. At this point, a built-in PCA function (e.g., Python: `sklearn.decomposition.pca`; Java: `weka.attributeSelection.PrincipalComponents`; Matlab: `pca`; R: `stats.princomp`) can also be used to compute the principal components U and the transformed *points* in the latent space.

First, the covariance matrix cov of the data matrix D is computed: $cov = \frac{1}{n-1}DD^T$. cov is a matrix of size c by c and D^T represents the transform of matrix D . Then, the *eigenvalues* and *eigenvectors* of cov are computed with a built-in function (e.g., Python: `numpy.linalg.eig`; Java: `org.apache.commons.math3.linear.EigenDecomposition`; Matlab: `eig`; R: `matlib.eigen`). The

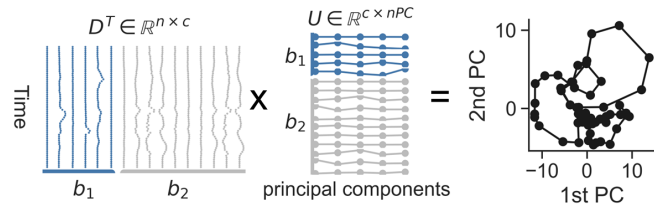


Figure 5: In principal component analysis (PCA), high-dimensional signals (left) are decomposed into its principal components (middle). Multiplying them results in the signals being translated to a lower-dimensional *latent space* (right), where signal redundancy and noise have been reduced and signal variability is maximized. The original time-domain biosignals D^T (left), or the transpose of matrix D , is a matrix with n rows representing time and c columns representing biosignal channels. The biosignal channels may represent multiple biosignals b_1 (blue), b_2 (grey). The principal components U (middle), is a matrix with c rows representing biosignal channels and nPC columns representing the number of principal components to extract. nPC is a parameter for the $\$B$ that must be tuned for a given dataset. In this figure, $nPC = 5$. Multiplying D^T with U will transform the high-dimensional signals in a lower-dimensional latent space (right) with n rows representing time and nPC columns representing the number of principal components. The right plot represents the transformed data plotted over the first two principal axes, which represent directions of greatest variance.

eigenvalue decomposition of the covariance matrix ensures that the data represented in the latent space contains no redundancies (i.e., all eigenvectors are linearly independent). Next, the *eigenvectors* are sorted column-wise in order corresponding from the largest *eigenvalue* to the smallest *eigenvalue*, such that the first column in the sorted eigenvectors corresponds to the largest eigenvalue and the second column in the sorted eigenvectors corresponds to the second-largest eigenvalue and so on. The sorting ensures that the first principal component transforms the original data matrix D such that the first principal component contains the data of maximum variance, the second principal component contains the data of second maximum variance, and so on. The principal components U are then defined as the first nPC columns of the sorted eigenvectors. nPC , or the number of principal components to keep, is a parameter that must be explored and defined by the prototyper when implementing $\$B$. Lastly, the transpose of the original data matrix D^T is multiplied with the principal components U (i.e., D^TU) and flattened into a one-dimensional vector *points* of length $nPC \times n$. The final vector *points* can be used to compare the templates T_i against the candidates gestures G through a point-by-point comparison.

3.2.4 Step 4: Compute Template with Best Score. Lastly, a candidate gesture G is compared against templates T to find a template match T' that minimizes the distance between the candidate and template *points*. First, the candidate gesture G is read-in, resampled, and normalized with Steps 1 and 2. Next, all biosignals b and channels c for the candidate gesture G are vertically concatenated such that G is a matrix with c rows and n columns, where c represents the total number of channels across all measured biosignal types, and n represents the number of resampled time points. Last, G is compared against each template T_i . For each template,

the principal component of the template U computed in Step 3 is read-in. Then, G is transformed to the template latent space via matrix multiplication ($G^T U$) and the resulting matrix is flattened into a one-dimensional vector *points* of length $nPC \times n$. Then, the gesture *points* can be compared against the template points T_i by computing the sum of the absolute value of the difference between the two (i.e., $d = \sum_k |points[k] - T_i[k]|, k = 1 \text{ to } nPC \times n$) [46]. The template with the smallest distance will be considered a match.

3.3 Why PCA as a Dimensionality Reduction Method?

For high-dimensional noisy signals like what is measured from biosignal interfaces, dimensionality reduction is a critical step for gesture recognition to reduce noise and redundancies between signals. For the \$B recognizer, we chose to apply principal component analysis (PCA), but there are other ways of reducing the dimensionality of the data and extracting relevant information from noisy data. Here, we briefly summarize our justification and compare PCA to other common dimensionality reduction methods.

First, what does it mean to reduce the dimensionality of a gesture? In touch-based gestures, the gesture results in a two-dimensional x, y points array over time. Both directions usually contain unique information relevant to gesture recognition. In biosignal gestures, sensors measure and collect multi-dimensional points over time. For example, even a ubiquitous sensor such as an accelerometer collects acceleration data over three channels: x, y , and z . If multiple sensors are used (e.g., an accelerometer on each body segment), the number of channels can increase significantly. To decrease the number of dimensions (i.e., channels) and decrease noise associated with biosignals, dimensionality reduction is a critical step in biosignal gesture recognition.

There are many ways to decrease noise and enhance the signal from high-dimensional data, including channel reduction and linear and non-linear dimensionality reduction methods. Channel reduction is perhaps the most straightforward way to reduce high-dimensional data. In channel reduction, channels whose largest amplitude signal falls below a certain threshold (e.g., 5% of the maximum amplitude measured for a given biosignal) are ignored when matching template gestures to candidate gestures [54]. For example, if an individual only uses their right hand for mid-air gestures, biosignals measured from the left side can be ignored. The method is simple to implement and eliminates channels that only contain noise. However, it is not possible to combine redundant information with this method. In contrast, linear (e.g., principal component analysis [24]) and non-linear (e.g., autoencoder [1, Ch 14]) dimensionality reduction methods compress high-dimensional data into a lower-dimensional *latent* space that reduces noise and combines channels with redundant information. Linear dimensionality reduction methods are generally faster to train and easier to implement compared to non-linear dimensionality methods; therefore, we chose PCA for \$B.

3.4 Limitations of the \$B Recognizer

As with any method, there are limitations to \$B that must be considered. First, because we apply the same transformation to the latent space for both the template and candidate gestures, \$B cannot account for mirrored gestures. For example, if an individual wants mirrored gestures to be recognized but only stores templates for

the right hand, \$B will not consider the same gesture performed with the left hand a match. Similarly, if the sensors are moved or placed in a different orientation (e.g., an accelerometer is rotated 90 degrees on the person’s wrist) without storing new templates, \$B will not recognize candidate gestures accurately.

One way to include rotation invariance in biosignal interfaces is by applying dimensionality reduction methods to the candidate and template gestures separately, such that the transformation from the high-dimensional space to the lower-dimensional latent space is specific to each candidate and template gesture. However, when we tried this in our preliminary analysis, we found large distances in the latent space between gestures with the same recognition label due to noise in the original biosignals affecting the transformation. Therefore, in \$B, we account for these variations by applying the same transformation to the template and candidate gestures. As long as we have templates of the individual performing mirrored gestures with both hands, \$B will correctly recognize the gestures. Conversely, this design choice also enables users to map mirrored gestures to two separate recognition labels. For example, a tap with the right and left index fingers could represent “select” and “duplicate”, respectively. This could be useful in scenarios where users have limited movement and want to maximize the number of labels associated with a small gesture set.

4 \$B Evaluation: Method

The goal of this evaluation is to compare the performance of \$B to other commonly used biosignal gesture recognizers, namely traditional machine learning with expert features (traditional ML) and deep learning. To ensure a diverse sample of gestures and to ensure that \$B is ability-inclusive [65, 66], we collected personalized gestures from participants with ($N = 26$) and without ($N = 8$) motor disabilities. Due to the promise of biosignal interfaces to enable accessible device input [74], we wanted to develop a recognizer that worked for both people with and without upper-body motor disabilities.

4.1 Participants

We recruited 26 participants with and 8 without upper-body motor disabilities from the greater ANONYMOUS community. While we were primarily interested in how \$B performs for people with motor disabilities, we wanted to additionally evaluate its performance on a small set of people without motor disabilities as well. Demographics for our participants are reported in Table 1.

Our participants with disabilities ($N = 26$) self-reported various motor disabilities that affected their ability to physically interact with technology including: spinal-cord injury (13), muscular dystrophy (3), peripheral neuropathy (3), essential tremor (3), and other disabilities (4). Participants’ average age and standard deviation since disability onset was 17 ± 15 years, with the minimum and maximum time since disability onset being 2 and 52 years, respectively. The average age and standard deviation of the participants, when their disability started, was 33 ± 20 , with some participants having their disability since birth and the oldest disability onset at 68 years. We quantified the level of disability of the participants using the *Quick Disabilities of the Arm, Shoulder and Hand* instrument (Quick DASH) [26]. Quick DASH is a shortened version of the full DASH instrument [25]. It provides a quantitative [0, 100] measure

Table 1: Participant Demographics

Characteristic	with disability (N = 26)	without disability (N = 8)
Age: yrs, mean \pm SD	50 \pm 18	27 \pm 8
Gender		
Woman	12	5
Non-Binary	2	0
Man	12	3
Race/Ethnicity		
White/Caucasian	24	4
Black/ African-American	2	0
Asian	1	4
Handedness		
Right-handed	20	6
Left-handed	2	2
Right-handed before disability onset, but now left-handed	4	N/A

of upper-body function, and greater values indicate that a disability has a greater impact on daily life¹. The average Quick DASH score and standard deviation was 55 \pm 18, with the minimum measured score being 14 and the maximum being 82.

4.2 Apparatus

We placed combined Delsys² EMG and IMU sensors on the participants' upper-body (Fig. 6). 12 inertial measurement unit (IMU) sensors were placed on participants' wrists, forearms, upper arms, shoulders, and neck to measure linear and rotational movement. 16 electromyography (EMG) sensors were placed on participants' finger muscles, forearm muscles, upper-arm muscles, and shoulder or neck muscles to measure muscle activations, which can occur without movement. Delsys Trigno Duo were placed on the smaller finger and forearm muscles and Delsys Trigno Avanti sensors were placed on the rest of the muscles. We used the Delsys software development kit to stream and save the biosignal data. The Avanti and Duo sensors collected IMU and EMG data at slightly different frequencies (Avanti: 74 Hz and 1259 Hz, respectively; Duo: 74 Hz and 1926 Hz, respectively). The software development kit synchronized all the data and upsampled the IMU signals to 148 Hz and the EMG signals to 2000 Hz. The data was collected using a customized data collection interface in Unity.³

¹We modified the wording of the Quick DASH to mitigate ableist assumptions that the person's disability is a *problem*. For example, one question asks "...to what extent has your arm, shoulder or hand *problem* interfered with your normal social activities...?" This was replaced with "...to what extent has your arm, shoulder or hand *affected* by your disability and/or chronic condition interfered with your normal social activities...?"

²Delsys, Inc., Boston, MA, USA. <https://delsys.com/>

³Unity Technologies, San Francisco, CA, USA. <https://unity.com/>

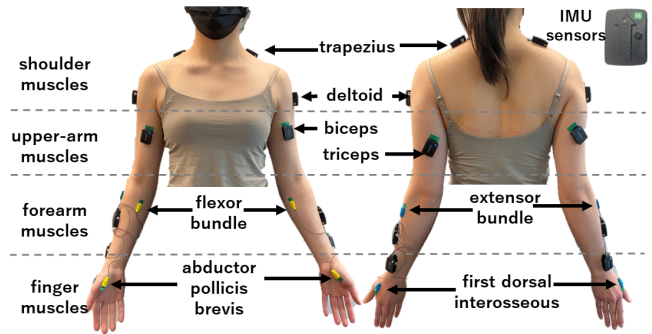


Figure 6: Combined IMU and EMG sensors were placed on the participant's shoulders (trapezius, deltoid) and upper arms (biceps, triceps). The large black sensors on the forearms and wrists only sense IMU signals. The small yellow and blue sensors on the person's forearms (flexor, extensor) and hands (abductor pollicis brevis, first dorsal interosseous) only sense EMG signals. The placements were chosen to sense movement or muscle activation from the participant's upper body, including the fingers, arms, shoulders, neck, and head. This figure was adapted from [74].

4.3 Procedure

Participants provided consent according to our protocol approved by the ANONYMOUS Institutional Review Board. Participants filled out a short demographics questionnaire that asked about their age, gender, race, ethnicity, and handedness. Participants with motor disabilities also reported on their disability, time since the onset of their disability or chronic condition that affects their ability to interact with technology, and answered questions from the Quick DASH instrument [26] to quantify the extent to which their upper body affects their everyday lives.

We then had our participants perform gestures for each of the three conditions below in sequence. We did not randomize conditions or repeated gestures due to concerns about participant dropout, time constraints, and participant cognitive ability concerns. To account for time and fatigue fluctuations, participants repeated one gesture (rotate) in the *Variations* condition, introducing natural variations in gesture data. Participants did 10 gestures for each prompted function. A "function" was an action a user might take with an interactive system, for example, *zoom-in*. We collected a total of 180 gestures from each participant, who completed each of the three conditions:

- (1) *Personalized*: Participants were asked to come up with 10 gestures corresponding to 10 functions originally proposed in Wobbrock et al. [68]: (1) *move*, (2) *select*, (3) *rotate*, (4) *delete*, (5) *pan*, (6) *close*, (7) *zoom-in*, (8) *zoom-out*, (9) *open*, (10) *duplicate*.⁴ Participants were told that they could come up with any gesture they wanted that involved their upper body, including their fingers, arms, shoulders, and head or neck.

⁴Two participants without disabilities were prompted to perform gestures for *shrink* and *enlarge* instead of *duplicate* and *open*. One participant performed the same gesture for *shrink* and *zoom-out*, as they felt that the two were identical functions. Both participants mentioned feeling as though *shrink/enlarge* and *zoom-in/zoom-out* were effectively the same functions. Therefore, we changed *shrink* and *enlarge* to *duplicate* and *open* for subsequent participants.

- (2) *Variations*: Participants were asked to articulate the *rotate* gesture in different ways to determine \$B's performance when the same gestures are articulated differently. We chose only one gesture to articulate in different ways to decrease fatigue and minimize our study duration. The *rotate* gesture was chosen because of its applicability in different situations, such as turning a wheel quickly in a virtual reality game or rotating a large image on a screen. At the beginning of the variations condition, each participant was shown a video of themselves performing their rotate gestures in the personalized phase to ensure they remembered the gesture they came up with. For the "time" variation, we asked participants to do the gesture in the same way they did in the personalized condition. This was to test the effect of fatigue and time on biosignals. For the "speed" variation, we asked participants to do the same rotate gesture, but as fast as possible. For the "size" variation, we asked participants to do the rotate gesture as large as possible.
- (3) *Standardized*: Participants were asked to perform five standardized gestures currently integrated into the Meta Oculus virtual reality platform [39] and Microsoft HoloLens augmented reality platform [41]: (1) *point and pinch*, (2) *pinch and scroll*, (3) *palm pinch*, (4) *air tap*, and (5) *wrist tap*. Items 1-4 are one-handed gestures, while item 5 is a two-handed gesture. For each gesture, participants were shown videos of an avatar performing the gesture. Participants without motor disabilities were asked to do the gesture exactly as shown in the video. Participants with motor disabilities could choose whichever hand they preferred to do one-handed gestures. Individuals whose disabilities only affected function on one side were asked to use their affected side to do the one-handed gestures.

Participants without motor disabilities ($N = 8$) completed all three conditions. All of our participants with motor disabilities ($N = 26$) completed the *personalized* condition, but only 25 and 10 participants completed the *variations* and *standardized* conditions, respectively. One participant did not complete the variations condition due to fatigue. Only 10 participants with motor disabilities fit our criteria of being able to touch their thumb and index finger together unassisted for the standardized condition. This inclusion criteria ensured that only participants who were physically able to do the standardized gestures were asked to do them.

4.4 Custom Gesture Segmentation

Biosignal-agnostic gesture segmentation is outside the scope of \$B and is an important area of future work. We implemented a custom gesture segmentation algorithm that automatically identified the beginning and end of a gesture using the raw EMG data. For each gesture, the experimenter prompted the participant to perform the gesture once data collection started; the experimenter stopped data collection after the gesture ended. This procedure resulted in signal padding at either end of the gesture. To remove this padding, we developed a pipeline that automatically identified where areas of activity (i.e., the gesture) started and ended.

For each gesture, we identified a subset of EMG channels that had a high amplitude, as well as EMG channels that had high variance. We chose to investigate the EMG channels rather than the IMU channels because prior work demonstrated that individuals with motor disabilities may flex their muscles without visibly moving [74]. This

meant that IMU data that relies on the sensor physically moving in space to record signals may not pick up the participants' subtle movements. With this subset of channels, we identified multiple candidate gesture start and end times through a combination of thresholding the signal based on the signal range [57] and differentiating the signal to identify large changes in slope. We removed candidate cutoffs that contributed to high variance within and between muscles as well as cutoffs that occurred in the wrong area of the signal (i.e., start times that occurred towards the end of the signal and end times that occurred towards the beginning of the signal). From the remaining candidate cutoffs, the first start cutoff and the last end cutoff were selected to ensure that only the gesture data was used for subsequent data analysis. The pseudocode for the custom gesture segmentation algorithm can be found in Appendix B.

4.5 Comparison Algorithms and Data Preprocessing

We tested \$B against two commonly used recognition methods in biosignal gesture recognition: (1) traditional machine learning with expert feature extraction (*traditional ML*) [2, 19, 31], and (2) *deep learning* [9, 32, 37, 71]. As these algorithms are not commonly used in HCI for biosignal data, we discuss them in more detail below.

As highlighted in previous sections, the two methods represent different expertise that is usually required for gesture recognition using biosignals. Expert feature extraction requires biosignal expertise, both the knowledge of which features to extract as well as how to implement the feature extraction in code. Some of the features can be complex and specific to the particular biosignal. Conversely, deep learning does not require biosignal expertise, as the deep learning algorithm will automatically learn the features that are most relevant to the recognition task. However, deep learning requires expertise in designing the model architecture, tuning hyperparameters, and writing and running the training code, which is a non-trivial task. Both methods require expertise in different ways that motivate the need for \$B to be implementable by non-experts.

4.5.1 Traditional ML. In *traditional ML*, features that are specific to specific biosignals and have previously been demonstrated to have discriminatory properties are extracted [2, 35]. Although EMG- and IMU-based interfaces are relatively new in HCI (and therefore, there is no consensus on what expert features are most suitable for HCI applications [21, 74]), feature extraction for EMG and IMU data has been extensively studied for prosthetic control [2, 35]. Therefore, we chose to implement expert features that have been validated to have high recognition accuracy for prosthetic hand control. Based on results from Abbaspour et al. [2], we chose 10 time-domain EMG features.⁵ Before the features were extracted, the raw EMG signals were filtered with a fourth-order Butterworth bandpass filter with a cutoff frequency of 10 Hz and 500 Hz [2]. We additionally computed six IMU features that were previously demonstrated to improve recognition accuracy compared to using solely EMG expert features [34].⁶ All features were computed over the entire time window in which the gesture occurred. Therefore, each gesture

⁵These features were mean absolute value, standard deviation, difference absolute mean value, integrated absolute value, variance, waveform length, correlation coefficient, Hjorth complexity parameter, and Hjorth mobility parameter.

⁶These features were the mean values of three accelerometer and three gyroscope outputs.

was distilled into 232 features total (10 EMG features \times 16 EMG sensors + 6 IMU features \times 12 IMU sensors). We used a multi-class support vector machine with a linear kernel for recognition. Hyperparameters were chosen based on performance during pilot testing.

4.5.2 Deep Learning. In *deep learning*, nonlinear models are used for feature extraction and gesture recognition [9, 37, 72]. Deep learning has recently been successfully applied to both prosthetic [9, 37] and HCI [72] gesture recognition tasks. The input data can be either expert features [37] or the biosignal data itself [9, 72]. Both simple (e.g., feedforward neural network [30]) and complex model architectures have been used (e.g., convolutional neural network [9], recurrent neural network [71], long-short term memory network [71]). In particular, prior work has demonstrated that extracting relevant biosignal features with a convolutional neural network (CNN) and then passing those features to a recurrent neural network such as a long-short term memory network (LSTM) results in high accuracy classifiers [32, 71]. Although we initially tested the three-layer one-dimensional CNN followed by a three-layer LSTM evaluated in Xie et al. [71], we found that shallower models resulted in better performance for the *Variations* condition during pilot testing. Therefore, we chose to implement a similar, but shallower deep learning model compared to Xie et al. [71].

Our final neural network consisted of a single-layer one-dimensional CNN followed by a two-layer LSTM and a feedforward neural network for classification. Before inputting the biosignal data into the CNN, we preprocessed the data as described below and followed the first two steps of \$B (resampling and normalizing) for better comparison. Therefore, the input to the CNN was the 88 normalized IMU and EMG channels resampled to 64 time points for a given gesture. A one-dimensional CNN was applied to this data with a kernel size of 2 and stride size of 1. The output was then passed to a two-layer LSTM with a hidden size of 64. Finally, a feedforward neural network with a hidden size of 64 was applied which outputted the number of classifications (ten for *Personalized* and *Variations*, five for *Standardized*). The rectified linear unit (ReLU) was used as the nonlinear activation for all layers. We used the Adam optimizer [33] with a learning rate of 0.001 and a batch size of 10 to train our neural network for each of the 20 epochs. Hyperparameters were chosen based on performance during pilot testing.

4.5.3 Data Preprocessing. We preprocessed the biosignal data that was the input to the \$B recognizer and the deep learning algorithm in the same way. For the IMU data, no pre-processing steps were applied as the data already had low noise and was collected at only 148 Hz. EMG data, on the other hand, was collected at 2000 Hz, and were stochastic and noisy; therefore, we computed the *EMG linear envelope* by filtering and downsampling. This pre-processing step provides a smooth trajectory that can be used as input to the algorithms. Following prior work analyzing upper-body EMG signals [73], we first filtered the EMG signal with a high-pass filter (fourth-order Butterworth filter at 40 Hz cutoff frequency), computed the absolute value of the EMG data, and then applied a low-pass filter (also a fourth-order Butterworth filter at 40 Hz cutoff frequency). We then downsampled the EMG data from 2000 Hz to 20 Hz by computing the moving average with a 100 ms window and a

50 ms overlap between windows. Although this step was necessary for our research-grade EMG system, which records unprocessed EMG signals, many EMG systems that are commercially available have the option to pre-compute the linear envelope [11, 56].

The IMU and EMG data were then read-in to \$B and deep learning algorithms. Our hyperparameters for \$B were time points per channel, $n = 64$ points, and number of principal components, $n_{PC} = 50$, which were chosen based on initial hyperparameter exploration.

4.6 Algorithm Evaluation

To compare \$B to *traditional ML* and *deep learning*, we adapted methods from Vatavu et al. [61], Wobbrock et al. [69] to compute user-dependent and user-independent recognition error rates. User-dependent error rates are computed individually for each participant. User-independent error rates are computed over multiple pooled participants.

First, we used the *personalized* and *variations* conditions to compute user-dependent recognition error rates. In these conditions, participants came up with gestures that were customized to their abilities. Similar to prior evaluations [61, 69], for each gesture type captured in the *personalized* condition, T samples were randomly chosen as templates, and 1 sample was chosen as the candidate gesture for recognition. The same template and candidate gestures were used for each of the three algorithms (\$B, traditional ML, deep learning). Additionally, 1 sample from each of the three *variations* conditions (time, speed, size) was chosen as a candidate gesture for recognition to test the effect of gesture articulation variability on recognition error rates. This process was repeated 100 times for each value of T , and the average accuracy was computed as the recognition error rate for each participant. We varied T from 1 template to 9 templates.

Second, we used the *standardized* condition to compute user-independent recognition error rates. As we had a limited dataset and we were interested in investigating algorithm recognition error rate differences between participants with and without motor disabilities, we performed a leave-one-out analysis, where all but one participant's data was used to train the models. For each of the 5 gesture types, T samples were randomly selected for each of the participants used for training. Then, one sample was chosen as a candidate gesture from the left-out "test participant" for recognition. This process was repeated 100 times for each participant. The average accuracy was computed as the recognition error rate for each participant. We varied T among three levels: small ($T = 1$), medium ($T = 3$), and large ($T = 7$) number of templates.

4.7 Experiment Design and Statistical Analysis

The primary reported outcome for all conditions was recognition error rate. The user-dependent data was generated from a mixed factorial design with the following factors and levels:

- *Algorithm* (within-subjects): \$B, traditional ML, deep learning;
- *Templates* (within-subjects): integers in the range [1-9];
- *Disability* (between-subjects): with, without.

When we examined the residuals from a $3 \times 9 \times 2$ mixed factorial repeated measures ANOVA, we found them non-normal according to the Shapiro-Wilk test [53]. After fitting various distributions to our residuals, we found that a Gamma regression model was the

best fit according to the Kolmogorov-Smirnov test [4, 55]. Therefore, we analyzed the user-dependent data with a mixed-effects Gamma regression model [12]. Our random factor was our participant’s ID to account for correlated responses from participants due to having within-subjects factors. Due to the presence of zeros in our dependent variable, recognition error rate, a constant shift of one (+1) was applied to the response [45], which does not affect our analysis but enables Gamma models to be fitted with their canonical “inverse” link function.

The gesture articulation variability data was similarly generated from a mixed factorial design with the same conditions as the user-dependent study, above, and with one additional factor:

- *Gesture Articulation* (within-subjects): time, speed, size

Similar to the user-dependent data, we found that our residuals were not normally distributed but followed a Gamma distribution. Therefore, we also analyzed the gesture articulation variability data with a mixed-effects Gamma regression model.

Lastly, the user-independent data was similarly generated from a mixed factorial design with the same conditions as the user-dependent study, above, but with only three levels of templates tested instead of nine:

- *Templates* (within-subjects): 1, 3, 7 templates

We again analyzed the user-independent data with a mixed-effects Gamma regression model.

Unless specified, reported values are mean (standard deviation) across participants and templates. For all three gesture conditions (user-dependent, gesture articulation variability, user-independent), we performed an analysis of variance using a mixed-effects Gamma regression model, which is a type of generalized linear mixed model (GLMM) [12]. Holm’s sequential Bonferroni procedure [28] was used to correct for multiple comparisons when performing *post hoc* tests on significant main and interaction effects.

We chose not to compare computing time as it varies depending on how algorithms are implemented. For example, the Python implementation of PCA is optimized to run more efficiently than if the principal components are computed by hand [20]. To ensure that our algorithm runs at interactive speeds (i.e., below 500 ms [5, 47]), we classified 100 gestures using \$B for one participant for the *personalized* condition. We chose to test the algorithm with three and nine templates, as a larger numbers of templates means slower run times because each template must be compared against the candidate gesture. We found that the mean and standard deviation run-time for three and nine templates was 235 ms ($SD=25$) and 485 ms ($SD=38$), respectively, reasonable for interactive use.

The complete dataset and analysis code is publicly available at ANONYMOUS.

5 \$B Evaluation: Results

We present the results from our evaluation of \$B, including the results from its user-dependent and user-independent evaluations. In addition, we also used the models developed from the user-dependent data to test the robustness of the three algorithms to substantial variability in gesture articulation.

5.1 User-Dependent Result: \$B Outperforms Traditional ML and Deep Learning

On average, the \$B recognizer outperformed the traditional ML and deep learning algorithms (Fig. 7a), with average recognition error rates of 9% ($SD=9$), 18% ($SD=13$), and 17% ($SD=14$), respectively, across the 10 personalized gestures ($\chi^2_{2,N=918} = 170.7, p < .0001$). *Post hoc* pairwise comparisons, corrected with Holm’s sequential Bonferroni procedure [28], indicated that all three algorithms had a significantly different recognition error rates ($p < .0001$).

Templates also had a significant main effect on recognition error rate for all tested algorithms ($\chi^2_{1,N=918} = 882.4, p < .0001$) While all three evaluated algorithms improve in recognition error rate as the number of training samples increase, the \$B recognizer performs well even with a few templates. The recognition error rate for \$B, traditional ML, and deep learning ranged from 22% ($SD=11$), 35% ($SD = 16$), and 42% ($SD=13$) with one training sample, respectively, to 5% ($SD=5$), 12% ($SD=8$), and 7% ($SD=6$) for nine training examples, respectively. \$B’s recognition error rate improves more modestly compared to traditional ML and deep learning, so there was an interaction effect between *Algorithm* and *Templates* ($\chi^2_{1,N=918} = 69.1, p < 0.0001$).

There were no main or interaction effects with *Disability*, suggesting that all three algorithms performed similarly across participants with and without disabilities ($\chi^2_{1,N=918} = 0.5, n.s.$).

5.2 Gesture Articulation Variability Result: \$B Performs Robustly

\$B performed robustly even when gesture articulation was varied across time, speed, and size⁷ (Fig. 7b) compared to traditional ML and deep learning ($\chi^2_{2,N=2673} = 192.7, p < .0001$). *Post hoc* pairwise comparisons showed all three algorithms were significantly different from each other ($p < .0001$), with \$B the best. There was also a significant effect of *Gesture Articulation* on recognition error rate ($\chi^2_{2,N=2673} = 15.7, p = .0004$). The gestures articulated at a different time had a lower recognition error rate than the gestures that were articulated at a different speed or at a different size ($p < .0001$).

The average recognition error rate for \$B, traditional ML, and deep learning algorithms when the *rotate* gesture was performed at a different time was 18% ($SD = 26$), 55% ($SD=32$), and 33% ($SD = 27$), respectively. As fatigue [17] and the length of time that a wearable sensor is placed on the user’s body [73] can affect the biosignal amplitude, this result suggests that \$B performs robustly despite these time-based biosignal fluctuations. Similarly, \$B’s performance extrapolated well when *rotate* was performed at a different speed and size that was not included in the training dataset (speed: 28% ($SD=34$), size: 25% ($SD=33$)) compared to the traditional ML (speed: 64% ($SD=30$), size: 67% ($SD=33$)) and deep learning (speed: 50% ($SD=25$), size: 50% ($SD=31$)). As the number of templates increased, the recognition error rate improved for all three algorithms ($\chi^2_{1,N=2673} = 55.1, p < .0001$).

⁷Recall that for the “time” variation, we asked participants to make the *rotate* gesture in the same way they did in the *personalized* condition to test the effect of time between gestures. For the “speed” variation, we asked participants to perform the gesture as fast as possible. For the “size” variation, we asked participants to perform the gesture as large as possible.

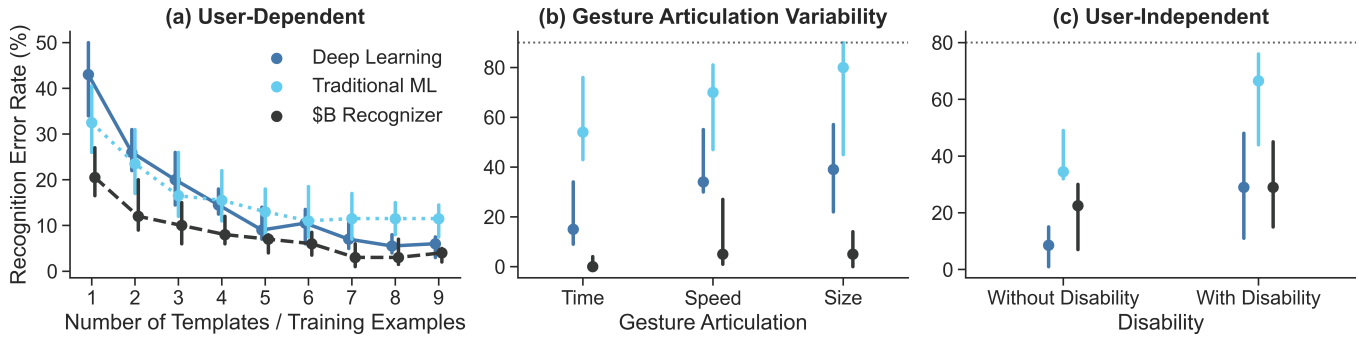


Figure 7: Recognition error rate comparison between \$B (black), traditional ML (light blue), and deep learning (dark blue). All Y-axes are recognition error rate, where lower values indicate greater accuracy. Medians are plotted with 25/75 percentile error bars. (a) The effect of Templates on user-dependent recognition error rate. As there are 10 possible gesture classes, the pure chance error rate is 90% (not shown). (b) The effect of gesture articulation variability (by time, speed, size) on user-dependent models. As there are 10 possible gesture classes, the pure chance error rate is 90% (horizontal dotted gray line). Only the results from using the analysis with 7 templates are shown. (c) The effect of Disability on user-independent recognition error rate. As there are 5 possible gesture classes, the chance error is 80% (horizontal dotted gray line). Only the results from using the analysis with 7 templates are shown.

There was a marginal effect of *Disability* on the recognition error rate ($\chi^2_{1,N=2673} = 3.1, p = .08$), with the recognition error rate for non-disabled gestures at 33% ($SD=33$) and disabled gestures at 47% ($SD=34$). There was also an interaction between *Algorithm* and *Disability* ($\chi^2_{2,N=2673} = 29.8, p < .0001$). \$B and deep learning had a better recognition error rate for participants without disabilities than participants with disabilities (\$B: 23% ($SD=11$) versus 34% ($SD=23$), without and with disability, $p < .005$; deep learning: 12% ($SD=9$) versus 30% ($SD=18$), without and with disability, $p < .02$). Traditional ML had no significant difference in error recognition rates.

5.3 User-Independent Result: Both \$B and Deep Learning Perform Well for Participants with Disabilities

In our user-independent evaluations, deep learning outperformed both \$B and the traditional ML algorithm (Fig. 7c) ($\chi^2_{2,N=162} = 449.0, p < .0001$). *Post hoc* pairwise comparisons show all three algorithm performances were significantly different ($p < .0001$). The average recognition error rates for \$B, traditional ML, and deep learning were 29% ($SD=19$), 56% ($SD = 16$), and 22% ($SD = 17$), respectively. More templates resulted in an improved recognition error rate ($\chi^2_{2,N=162} = 10.4, p = .005$). There was a marginal main effect with *Disability* ($\chi^2_{1,N=162} = 3.2, p = .07$).

There was a significant interaction between *Algorithm* and *Disability* ($\chi^2_{2,N=162} = 9.2, p < .01$). There was a marginal effect of the deep learning algorithm performing better for participants without disabilities than participants with disabilities (without disability: 12% ($SD = 9$); with disability: 30% $SD = 18$); $p = .08$). Although deep learning outperformed \$B for participants without disabilities (deep learning: 12% ($SD = 9$); \$B: 23% ($SD = 11$); $p < .0001$), there was no difference in recognition error rate between the two algorithms for participants with disabilities (deep learning: 30% ($SD=18$); \$B: 34% ($SD = 23$); *n.s.*). There was also no significant difference in recognition error rate between participants with and without disabilities for \$B and traditional ML. This result shows that

\$B performs robustly across both user groups, whereas deep learning performs significantly better than \$B only for people without disabilities.

6 Discussion

Our evaluation suggests that the \$B recognizer performs well for personalized biosignal gesture recognition, with over 90% accuracy on average. In comparison, other algorithms typically deployed for biosignal gesture recognition, traditional machine learning using expert feature extraction (traditional ML) and deep learning, had 82% and 83% accuracy, respectively (with 10% chance accuracy). \$B performed well even with a small number of templates, and had a 78% accuracy with one template compared to 65% and 58% for the traditional ML and deep learning algorithms, respectively. Similarly, \$B performed well even with gesture articulation variability, and had 76% accuracy compared to 38% and 56% accuracy for the traditional ML and deep learning algorithms, respectively. Although deep learning outperformed \$B overall for user-independent evaluations, both algorithms performed comparably for participants with disabilities (deep learning: 70%; \$B: 66% recognition accuracy). Our results highlight \$B's success in accurately recognizing biosignal gestures despite a small number of templates and variability in gesture articulation, especially for participants with motor disabilities.

6.1 \$B's Recognition Rate is Comparable to State-of-the-Art

\$B's accuracy is comparable to other work that recognizes biosignal gestures using user-dependent models. For example, EMG gesture recognizers from Ctrl-Labs at Reality Labs [16] had a recognition accuracy between 49% and 73% across 100 participants without disabilities and nine gesture classes (with 11% chance accuracy), and Krasoulis et al. [35] had a recognition accuracy between 70% and 95% across 12 participants without disabilities and 2 trans-radial amputees and five gesture classes (with 20% chance accuracy). Comparing our results against prior work that employed few-shot learning to personalize gestures for participants without disabilities, our work performs comparably. For example, Xu et al. [72] found a 55%, 83%, and 87% gesture recognition accuracy with one,

three, and five templates across 12 new gesture classes (with 8.3% chance accuracy). Shahi et al. [52] found 95% gesture recognition accuracy with four templates across four new gesture classes (with 25% chance accuracy). In comparison, \$B had a comparable gesture recognition accuracy of 91% and 93% with four and five templates across 10 gesture classes (with 10% chance accuracy), without the need for a large dataset or advanced learning methods.

Similarly, \$B is robust to variations in gesture articulation variability, whether that be due to changes in the biosignal due to time, speed, or size, with an average accuracy of 76% compared to 38% and 56% for the traditional ML and deep learning algorithms, respectively. An interesting finding was that both traditional ML and deep learning algorithms performed poorly when the same gesture was performed at a different time. This may be because participants became fatigued throughout the study, and by the time they repeated the gesture, they performed the gesture differently (e.g., slower, smaller, or with less vigor). Another reason may be due to changes in the EMG signal itself. Prior work has shown that EMG impedance decreases over several hours after the sensor is placed [73], and EMG signals also change with fatigue [17]. Therefore, algorithms must be resilient to time-based changes in biosignal variability. In our work, we ensured that time-based fluctuations in biosignals do not affect gesture recognition by normalizing the biosignals so that the total standard deviation across all channels for a given biosignal is equal to one [30].

For our user-dependent evaluation, the largest dataset the algorithms had access to was 9 templates \times 10 gestures = 90 gestures. For our user-independent evaluation, the largest dataset the algorithms had access to was 7 templates \times 5 gestures \times 17 participants = 595 gestures. The order of magnitude increase in dataset size appeared to significantly improve the gesture recognition accuracy for deep learning for participants without disabilities. However, we did not see a similar improvement in performance for participants with motor disabilities. Both \$B and deep learning performed comparably, with 66% and 70% recognition accuracy, respectively. This result suggests that for users with larger gesture articulation heterogeneity (such as for users with motor disabilities), \$B will continue to perform comparably to other recognizers, as it is more robust to gesture articulation variability.

Qualitatively, we observed differences in how the standardized gestures were articulated between participants with and without disabilities. First, all participants without disabilities performed their gestures mid-air at chest height, while participants with motor disabilities tended to perform their gestures at waist level, with their hands resting on or barely above their armchair. Second, all participants without disabilities performed the standardized gestures exactly as demonstrated, whereas participants with motor disabilities could choose whichever hand they preferred to do one-handed gestures. This meant that participants with disabilities who performed the standardized gesture with the opposite hand than what was demonstrated had fewer training examples. Third, participants with disabilities tended to perform the standardized gestures more slowly and smaller than participants without disabilities.

6.2 Limitations

One limitation of \$B is classifying gestures across participants without disabilities. For participants without disabilities, deep learning

outperformed \$B by 11% in the user-independent evaluation. Similarly, comparing \$B's user-independent recognition accuracy with other work that generalized models across participants, \$B's overall gesture recognition accuracy of 71% across five gesture classes (with 25% chance accuracy) was slightly lower than other work. For example, Xu et al. [72] had a 96% accuracy across four gesture classes and over 500 participants. Ctrl-Labs at Reality Labs [16] had a 93% accuracy across seven gesture classes and over 6,500 participants. These results highlight the strength of deep learning with much larger datasets [16].

Another limitation with \$B is that recognition speed decreases as more templates are added, as each template will have to be compared against the candidate gesture. We do not anticipate this to be an issue for personalized biosignal gesture interfaces as users will save a small number of templates, but it could be a challenge for user-independent applications, where there may be many templates saved from different users. Future work should consider additions to \$B that speed up the recognition, similar to how \$Q [62] significantly improved computing resources and time compared to \$1 [69] and \$P [61].

Finally, compared to prior \$-family recognizers, \$B achieved a lower gesture recognition accuracy overall. The original \$1 unistroke recognizer had over 99% accuracy, and the \$P multistroke recognizer had over 95% accuracy. In comparison, multiple studies have demonstrated that biosignal gesture recognition ranges from 50% [16] to 95% [35] for user-dependent algorithms. These recognition rates are despite years of sustained work on developing better expert features [2] and deep learning architectures [16, 59]. In our evaluation, \$B had a recognition accuracy of 95% with only nine templates, on the upper-end of this scale. This gap in accuracy highlights the challenge of recognizing multi-dimensional biosignal gestures compared to 2-D uni- or multistroke gestures. To close this gap, new innovations must be made in multi-dimensional biosignal gesture recognition for HCI applications.

7 Future Work: Towards a New Paradigm for Biosignal Gesture Recognition in HCI

As highlighted in Eddy et al. [21], biosignal interfaces like electromyography, accelerometers, and depth camera interfaces are rapidly being applied for HCI applications both for users with [23, 42, 74] and without [16, 52, 72] disabilities. As many of these biosignals have been previously studied in-depth in areas like assistive technology [2, 9, 31, 37, 59] and rehabilitation [19, 27, 58], HCI biosignals research have tended to replicate the methods used in these fields [21]. For example, uninterrupted gesture recognition using a few hundred-millisecond windows is a common method in assistive technology for gesture classification [2, 9, 31, 37, 59]. This is because in prosthetics research, for example, gestures must be made continuously recognized to determine what position the prosthetic hand should be in at any given moment (e.g., open hand, close hand, flex hand, extend hand) [2]. However, uninterrupted gesture recognition may not be desirable in HCI applications because technology interactions are often intermittent. Additionally, recognizing gestures over sliding time windows makes it more challenging to identify gestures that are performed at different speeds, such as when users with motor disabilities perform gestures slower than users without disabilities. To account for these different needs

in HCI compared to body-machine interface research, we chose to recognize the entire gesture trajectory rather than continuously recognizing sliding time windows gestures.

Recognizing the entire gesture trajectory instead of sliding time windows poses new research questions for biosignal interfaces that were not considered in this work. First, what biosignal features should be used to identify the beginning and end of a gesture and ensure that naturalistic motions such as walking or cooking do not trigger a gesture classification? With a 2-D stroke interface, the beginning and end of a gesture are defined as when the person's pen or finger comes into physical contact with the screen. With mid-air gestures, there are no clear ways to determine when a person begins and ends a gesture. This highlights the need for new algorithms that can detect when people intend to interact with their technology [51].

Similarly, extracting expert features from biosignals data (e.g., mean absolute value, average signal power) is a powerful way to ensure that gesture classifiers are robust to natural fluctuations in biosignals [2, 37]. However, expert features that work well for assistive technology applications may not work well for HCI applications, especially if the time window over when the features are computed is over the entire gesture window rather than every few hundred milliseconds. Future work should consider what features should be extracted for biosignal interfaces in HCI. Our work builds on and emphasizes the call to action originally put forth by Eddy et al. [21] that new advances in sensors and algorithms are needed to fully integrate biosignals for HCI applications.

8 Conclusion

The \$B recognizer is a simple and effective algorithm that recognizes personalized gestures performed by participants with and without motor disabilities, with a recognition accuracy of over 95% with 9 templates. It performs well with only a few training samples (78% accuracy with 1 template) and recognizes gestures that are articulated in different ways or are articulated by different people. The accuracy is comparable to other work that classifies biosignal gestures and outperformed algorithms that require domain expertise in biosignals (traditional machine learning using expert feature extraction) or algorithm development (deep learning). Similarly to how the \$-family recognizers transformed 2-D stroke gesture recognition, we hope that \$B makes it easier to integrate biosignal gesture recognition into next-generation user interface prototypes.

Acknowledgments

Anonymized for review.

References

- [1] 2016. Chapter 14: Autoencoders. In *Deep Learning*. Ian Goodfellow, Yoshua Bengio, and Aaron Courville (Eds.). MIT Press, 499–523.
- [2] Sara Abbaspour, Maria Lindén, Hamid Gholamhosseini, Autumn Naber, and Max Ortiz-Catalan. 2020. Evaluation of surface EMG-based recognition algorithms for decoding hand movements. *Med. Biol. Eng. Comput.* 58, 1 (Jan. 2020), 83–100.
- [3] Niccolò Albertini, Andrea Brogni, Riccardo Olivito, Emanuele Taccola, Baptiste Caramiaux, and Marco Gillies. 2017. Designing natural gesture interaction for archaeological data in immersive environments. *Virtual Archaeol. Rev.* 8, 16 (May 2017), 12.
- [4] Kolmogorov An. 1933. Sulla determinazione empirica di una legge didistribuzione. *Giorn Dell'inst Ital Degli Att* 4 (1933), 89–91.
- [5] Glen Anderson, Rina Doherty, and Subhashini Ganapathy. 2011. User Perception of Touch Screen Latency. In *Design, User Experience, and Usability. Theory, Methods, Tools and Practice*. Springer Berlin Heidelberg, 195–202.
- [6] Lisa Anthony and J Wobbrock. 2010. A lightweight multistroke recognizer for user interface prototypes. *Proc. Graph. Interface* (May 2010), 245–252.
- [7] Lisa Anthony and J Wobbrock. 2012. \$N-protractor: a fast and accurate multistroke recognizer. *Proc. Graph. Interface* (May 2012), 117–120.
- [8] Apple Support. [n. d.]. Use AssistiveTouch on your Apple Watch. <https://support.apple.com/en-us/111111>. Accessed: 2024-3-13.
- [9] Manfredo Atzori, Matteo Cognolato, and Henning Müller. 2016. Deep learning with convolutional neural networks applied to electromyography data: A resource for the classification of movements for prosthetic hands. *Front. Neurobot.* 10, SEP (2016), 1–10.
- [10] Joseph Berman, Robert Hinson, I-Chieh Lee, and He Huang. 2023. Harnessing Machine Learning and Physiological Knowledge for a Novel EMG-Based Neural-Machine Interface. *IEEE Trans. Biomed. Eng.* 70, 4 (April 2023), 1125–1136.
- [11] Backyard Brains. 2017. Muscle SpikerShield Bundle. <https://backyardbrains.com/products/muscleSpikershieldBundle>. Accessed: 2024-2-13.
- [12] N E Breslow and D G Clayton. 1993. Approximate Inference in Generalized Linear Mixed Models. *J. Am. Stat. Assoc.* 88, 421 (March 1993), 9–25.
- [13] P Carrington, J M Chang, K Chang, and others. 2016. The gest-rest family: Exploring input possibilities for wheelchair armrests. *ACM Transactions on* (2016).
- [14] Patrick Carrington, Amy Hurst, and Shaun K Kane. 2014. Wearables and chairables: Inclusive design of mobile input and output techniques for power wheelchair users. *Conference on Human Factors in Computing Systems - Proceedings Figure 1* (2014), 3103–3112.
- [15] Thomas H Cormen, Charles E Leiserson, Ronald L Rivest, and Clifford Stein. 2022. *Introduction to Algorithms, fourth edition*. MIT Press.
- [16] Ctrl-Labs at Reality Labs. 2024. A generic noninvasive neuromotor interface for human-computer interaction. (Feb. 2024), 2024.02.23.581779 pages.
- [17] C J De Luca. 1997. The Use of Surface Electromyography in Biomechanics. *Journal of Applied Biomechanics* 1, 13 (May 1997), 135–163.
- [18] Carlo J De Luca, L Donald Gilmore, Mikhail Kuznetsov, and Serge H Roy. 2010. Filtering the surface EMG signal: Movement artifact and baseline noise contamination. *J. Biomech.* 43, 8 (May 2010), 1573–1579.
- [19] Omid Dehzangi and Vaishali Sahu. 2018. IMU-Based Robust Human Activity Recognition using Feature Analysis, Extraction, and Reduction. In *2018 24th International Conference on Pattern Recognition (ICPR)*. IEEE, 1402–1407.
- [20] Scikit-Learn Developers. [n. d.]. [sklearn.decomposition.PCA](https://scikit-learn.org/stable/modules/generated/sklearn.decomposition.PCA.html). <https://scikit-learn.org/stable/modules/generated/sklearn.decomposition.PCA.html>. Accessed: 2024-3-29.
- [21] Ethan Eddy, Erik J Scheme, and Scott Bateman. 2023. A Framework and Call to Action for the Future Development of EMG-Based Input in HCI. In *Proceedings of the 2023 CHI Conference on Human Factors in Computing Systems* (Hamburg, Germany) (CHI '23, Article 145). Association for Computing Machinery, New York, NY, USA, 1–23.
- [22] Mingming Fan, Zhen Li, and Franklin Mingzhe Li. 2020. Eyelid Gestures on Mobile Devices for People with Motor Impairments. In *Proceedings of the 22nd International ACM SIGACCESS Conference on Computers and Accessibility* (Virtual Event, Greece) (ASSETS '20, Article 15). Association for Computing Machinery, New York, NY, USA, 1–8.
- [23] Rachel L Franz, Jinghan Yu, and Jacob O Wobbrock. 2023. Comparing Locomotion Techniques in Virtual Reality for People with Upper-Body Motor Impairments. In *Proceedings of the 25th International ACM SIGACCESS Conference on Computers and Accessibility* (<conf-loc>, <city>New York</city>, <state>NY</state>, <country>USA</country>, </conf-loc>) (ASSETS '23, Article 39). Association for Computing Machinery, New York, NY, USA, 1–15.
- [24] Michael Greenacre, Patrick J F Groenen, Trevor Hastie, Alfonso Iodice D'Enza, Angelos Markos, and Elena Tuzhilina. 2022. Principal component analysis. *Nature Reviews Methods Primers* 2, 1 (Dec. 2022), 1–21.
- [25] Christina Gummesson, Isam Atroshi, and Charlotte Ekdahl. 2003. The disabilities of the arm, shoulder and hand (DASH) outcome questionnaire: longitudinal construct validity and measuring self-rated health change after surgery. *BMC Musculoskelet. Disord.* 4 (June 2003), 11.
- [26] Christina Gummesson, Michael M Ward, and Isam Atroshi. 2006. The shortened disabilities of the arm, shoulder and hand questionnaire (QuickDASH): validity and reliability based on responses within the full-length DASH. *BMC Musculoskelet. Disord.* 7 (May 2006), 44.
- [27] N S K Ho, K Y Tong, X L Hu, K L Fung, X J Wei, W Rong, and E A Susanto. 2011. An EMG-driven exoskeleton hand robotic training device on chronic stroke subjects: task training system for stroke rehabilitation. *IEEE Int. Conf. Rehabil. Robot.* 2011 (2011), 5975340.
- [28] Sture Holm. 1979. A Simple Sequentially Rejective Multiple Test Procedure. *Scand. Stat. Theory Appl.* 6, 2 (1979), 65–70.
- [29] Donny Huang, Xiaoyi Zhang, T Scott Saponas, James Fogarty, and Shyamnath Gollakota. 2015. Leveraging dual-observable input for fine-grained thumb interaction using forearm EMG. *UIST 2015 - Proceedings of the 28th Annual ACM Symposium on User Interface Software and Technology* (2015), 523–528.

- [30] Nafe Muhtasim Hye, Umma Hany, Sumit Chakravarty, Lutfa Akter, and Imtiaz Ahmed. 2023. Artificial Intelligence for sEMG-Based Muscular Movement Recognition for Hand Prosthesis. *IEEE Access* 11 (2023), 38850–38863.
- [31] Nisheena V Iqbal, Kamalraj Subramaniam, and Shaniba Asmi P. 2018. A Review on Upper-Limb Myoelectric Prosthetic Control. *IETE J. Res.* 64, 6 (Nov. 2018), 740–752.
- [32] Naveen Kumar Karnam, Shiv Ram Dubey, Anish Chand Turlapaty, and Balakrishna Gokaraju. 2022. EMGHandNet: A hybrid CNN and Bi-LSTM architecture for hand activity classification using surface EMG signals. *Biocybernetics and Biomedical Engineering* 42, 1 (Jan. 2022), 325–340.
- [33] Diederik P Kingma and Jimmy Ba. 2014. Adam: A Method for Stochastic Optimization. (Dec. 2014). arXiv:1412.6980 [cs.LG]
- [34] Agamemnon Krasoulis, Iris Kyranou, Mustapha Suphi Erden, Kianoush Nazarpour, and Sethu Vijayakumar. 2017. Improved prosthetic hand control with concurrent use of myoelectric and inertial measurements. *J. Neuroeng. Rehabil.* 14, 1 (July 2017), 71.
- [35] Agamemnon Krasoulis, Sethu Vijayakumar, and Kianoush Nazarpour. 2020. Multi-Grip Classification-Based Prosthesis Control With Two EMG-IMU Sensors. *IEEE Trans. Neural Syst. Rehabil. Eng.* 28, 2 (Feb. 2020), 508–518.
- [36] Franklin Mingzhe Li, Michael Xieyang Liu, Yang Zhang, and Patrick Carrington. 2022. Freedom to Choose: Understanding Input Modality Preferences of People with Upper-body Motor Impairments for Activities of Daily Living. In *ASSETS 2022 - Proceedings of the 24th International ACM SIGACCESS Conference on Computers and Accessibility*. Association for Computing Machinery, Inc.
- [37] Wei Li, Ping Shi, and Hongliu Yu. 2021. Gesture Recognition Using Surface Electromyography and Deep Learning for Prostheses Hand: State-of-the-Art, Challenges, and Future. *Front. Neurosci.* 15 (April 2021), 621885.
- [38] Meethu Malu, Pramod Chundury, and Leah Findlater. 2018. Exploring Accessible Smartwatch Interactions for People with Upper Body Motor Impairments. In *Proceedings of the 2018 CHI Conference on Human Factors in Computing Systems* (Montreal QC, Canada) (CHI '18, Paper 488). Association for Computing Machinery, New York, NY, USA, 1–12.
- [39] Meta. [n.d.]. Getting started with Hand Tracking on Meta Quest headsets. <https://www.meta.com/help/quest/articles/headsets-and-accessories/controllers-and-hand-tracking/hand-tracking/>. Accessed: 2024-1-24.
- [40] Antigoni Mezari and Ilias Maglogiannis. 2018. An Easily Customized Gesture Recognizer for Assisted Living Using Commodity Mobile Devices. *J. Healthc. Eng.* 2018 (July 2018), 3180652.
- [41] Microsoft. 2021. HoloLens 2 gestures for authoring/navigating in Dynamics 365 Guides - Dynamics 365 Mixed Reality. <https://learn.microsoft.com/en-us/dynamics365/mixed-reality/guides/authoring-gestures-hl2>. Accessed: 2024-1-24.
- [42] Claire L Mitchell, Gabriel J Cler, Susan K Fager, Paola Contessa, Serge H Roy, Gianluca De Luca, Joshua C Kline, and Jennifer M Vojtech. 2022. Ability-based keyboards for augmentative and alternative communication: Understanding how individuals' movement patterns translate to more efficient keyboards: Methods to generate keyboards tailored to user-specific motor abilities. *Ext. Abstr. Hum. Factors Computing Syst.* 2022 (April 2022).
- [43] Martez Mott, John Tang, Shaun Kane, Edward Cutrell, and Meredith Ringel Morris. 2020. "I just went into it assuming that I wouldn't be able to have the full experience": Understanding the Accessibility of Virtual Reality for People with Limited Mobility. In *Proceedings of the 22nd International ACM SIGACCESS Conference on Computers and Accessibility* (<conf-loc>, <city>Virtual Event</city>, <country>Greece</country>, </conf-loc>) (ASSETS '20, Article 43). Association for Computing Machinery, New York, NY, USA, 1–13.
- [44] Miguel A Nacenta, Yemliha Kamber, Yizhou Qiang, and Per Ola Kristensson. 2013. Memorability of pre-designed and user-defined gesture sets. In *Proceedings of the SIGCHI Conference on Human Factors in Computing Systems* (Paris, France) (CHI '13). Association for Computing Machinery, New York, NY, USA, 1099–1108.
- [45] Jason Osborne. 2002. Notes on the use of data transformations. *Practical assessment, research, and evaluation* 8, 1 (2002).
- [46] Phillip T Pasqual and Jacob O Wobbrock. 2014. Mouse pointing endpoint prediction using kinematic template matching. In *Conference on Human Factors in Computing Systems - Proceedings*. Association for Computing Machinery, 743–752.
- [47] Walter Ritter, Guido Kempter, and Tobias Werner. 2015. User-Acceptance of Latency in Touch Interactions. In *Universal Access in Human-Computer Interaction. Access to Interaction*. Springer International Publishing, 139–147.
- [48] Fabio Rizzoglio, Maura Casadio, Dalia De Santis, and Ferdinando A Mussa-Ivaldi. 2021. Building an adaptive interface via unsupervised tracking of latent manifolds. *Neural Netw.* 137 (May 2021), 174–187.
- [49] Dean Rubine. 1991. Specifying gestures by example. *SIGGRAPH Comput. Graph.* 25, 4 (July 1991), 329–337.
- [50] T Scott Saponas, Desney S Tan, Dan Morris, and Ravin Balakrishnan. 2008. Demonstrating the feasibility of using forearm electromyography for muscle-computer interfaces. *Proceeding of the twenty-sixth annual CHI conference on Human factors in computing systems CHI 08 00* (2008), 515.
- [51] Julia Schwarz, Charles Claudius Marais, Tommer Leyvand, Scott E Hudson, and Jennifer Mankoff. 2014. Combining body pose, gaze, and gesture to determine intention to interact in vision-based interfaces. In *Proceedings of the SIGCHI Conference on Human Factors in Computing Systems* (Toronto, Ontario, Canada) (CHI '14). Association for Computing Machinery, New York, NY, USA, 3443–3452.
- [52] Soroush Shahi, Cori Tymoszek Park, Richard Kang, Asaf Liberman, Oron Levy, Jun Gong, Abdelkareem Bedri, and Gierad Laput. 2024. Vision-Based Hand Gesture Customization from a Single Demonstration. (Feb. 2024). arXiv:2402.08420 [cs.HC]
- [53] S S Shapiro and M B Wilk. 1965. An analysis of variance test for normality (complete samples). *Biometrika* 52, 3-4 (Dec. 1965), 591–611.
- [54] Adwait Sharma, Christina Salchow-Hömmen, Vimal Suresh Mollyn, Aditya Shekhar Nittala, Michael A Hedderich, Marion Koelle, Thomas Seel, and Jürgen Steimle. 2023. SparseIMU: Computational Design of Sparse IMU Layouts for Sensing Fine-grained Finger Microgestures. *ACM Trans. Comput.-Hum. Interact.* 30, 3 (June 2023), 1–40.
- [55] N Smirnov. 1939. Sur les écarts de la courbe de distribution empirique: Recueil Mathématique (Matematicheskii Sbornik), v. *New Solut.* 6 (1939), 3–26.
- [56] SparkFun. 2023. MyoWare 2.0 Muscle Sensor. <https://www.sparkfun.com/products/21265>. Accessed: 2024-2-13.
- [57] Gerhard Staude, Claus Flachenecker, Martin Daumer, and Werner Wolf. 2001. Onset Detection in Surface Electromyographic Signals: A Systematic Comparison of Methods. *EURASIP J. Adv. Signal Process.* 2001, 2 (June 2001), 1–15.
- [58] Dongnan Su, Zhigang Hu, Jipeng Wu, Peng Shang, and Zhaohui Luo. 2023. Review of adaptive control for stroke lower limb exoskeleton rehabilitation robot based on motion intention recognition. *Front. Neurobot.* 17 (July 2023), 1186175.
- [59] Triwiyanto Triwiyanto, Wahyu Caesarendra, Abdussalam Ali Ahmed, and V H Abdullayev. 2023. How Deep Learning and Neural Networks can Improve Prosthetics and Exoskeletons: A Review of State-of-the-Art Methods and Challenges. *Journal of Electronics, Electromedical Engineering, and Medical Informatics* 5, 4 (Oct. 2023), 277–289.
- [60] Radu-Daniel Vatavu. 2017. Improving Gesture Recognition Accuracy on Touch Screens for Users with Low Vision. In *Proceedings of the 2017 CHI Conference on Human Factors in Computing Systems* (Denver, Colorado, USA) (CHI '17). Association for Computing Machinery, New York, NY, USA, 4667–4679.
- [61] Radu-Daniel Vatavu, Lisa Anthony, and Jacob O Wobbrock. 2012. Gestures as point clouds: a \$P\$ recognizer for user interface prototypes. In *Proceedings of the 14th ACM international conference on Multimodal interaction* (Santa Monica, California, USA) (ICMI '12). Association for Computing Machinery, New York, NY, USA, 273–280.
- [62] Radu-Daniel Vatavu, Lisa Anthony, and Jacob O Wobbrock. 2018. \$Q\$: a super-quick, articulation-invariant stroke-gesture recognizer for low-resource devices. In *Proceedings of the 20th International Conference on Human-Computer Interaction with Mobile Devices and Services* (Barcelona, Spain) (MobileHCI '18, Article 23). Association for Computing Machinery, New York, NY, USA, 1–12.
- [63] Radu Daniel Vatavu and Ovidiu Ciprian Ungurean. 2022. Understanding Gesture Input Articulation with Upper-Body Wearables for Users with Upper-Body Motor Impairments. In *Conference on Human Factors in Computing Systems - Proceedings*. Association for Computing Machinery.
- [64] Yaqing Wang, Quanming Yao, James T Kwok, and Lionel M Ni. 2020. Generalizing from a Few Examples: A Survey on Few-shot Learning. *ACM Comput. Surv.* 53, 3 (June 2020), 1–34.
- [65] Jacob O Wobbrock, Krzysztof Z Gajos, Shaun K Kane, and Gregg C Vanderheiden. 2018. Ability-based design. *Commun. ACM* 61, 6 (May 2018), 62–71.
- [66] Jacob O Wobbrock, Shaun K Kane, Krzysztof Z Gajos, Susumu Harada, and Jon Froehlich. 2011. Ability-Based Design. *ACM Trans. Access. Comput.* 3, 3 (2011), 1–27.
- [67] Jacob O Wobbrock and Julie A Kientz. 2016. Research contributions in human-computer interaction. *Interactions* 23, 3 (April 2016), 38–44.
- [68] Jacob O Wobbrock, Meredith Ringel Morris, and Andrew D Wilson. 2009. User-defined gestures for surface computing. *Conference on Human Factors in Computing Systems - Proceedings* (2009), 1083–1092.
- [69] Jacob O Wobbrock, Andrew D Wilson, and Yang Li. 2007. Gestures without Libraries, Toolkits or Training: A \$I\$ Recognizer for User Interface Prototypes. In *Proceedings of the 20th Annual ACM Symposium on User Interface Software and Technology*. Association for Computing Machinery, New York, NY, USA, 159–168.
- [70] Huiyue Wu, Shaoke Zhang, Jiayi Liu, Jiali Qiu, and Xiaolong (luke) Zhang. 2019. The Gesture Disagreement Problem in Free-hand Gesture Interaction. *International Journal of Human-Computer Interaction* 35, 12 (July 2019), 1102–1114.
- [71] Baao Xie, Baihua Li, and Andy Harland. 2018. Movement and Gesture Recognition Using Deep Learning and Wearable-sensor Technology. In *Proceedings of the 2018 International Conference on Artificial Intelligence and Pattern Recognition* (Beijing, China) (AIPR '18). Association for Computing Machinery, New York, NY, USA, 26–31.
- [72] Xuhai Xu, Jun Gong, Carolina Brum, Lilian Liang, Bongsoo Suh, Shivam Kumar Gupta, Yash Agarwal, Laurence Lindsey, Runchang Kang, Behrooz Shahsavari, Tu Nguyen, Heriberto Nieto, Scott E Hudson, Charlie Maalouf, Jax Seyed Mousavi, and Gierad Laput. 2022. Enabling Hand Gesture Customization on Wrist-Worn

Devices. In *Conference on Human Factors in Computing Systems - Proceedings*. Association for Computing Machinery.

- [73] Momona Yamagami, Keshia M Peters, Ivana Milovanovic, Irene Kuang, Zeyu Yang, Nanshu Lu, and Katherine M Steele. 2018. Assessment of dry epidermal electrodes for long-term electromyography measurements. *Sensors* 18, 4 (2018), 1–15.
- [74] Momona Yamagami, Alexandra A Portnova-Fahreva, Junhan Kong, Jacob O Wobbrock, and Jennifer Mankoff. 2023. How Do People with Limited Movement Personalize Upper-Body Gestures? Considerations for the Design of Personalized and Accessible Gesture Interfaces. In *Proceedings of the 25th International ACM SIGACCESS Conference on Computers and Accessibility* (New York, NY, USA) (*ASSETS '23, Article 1*). Association for Computing Machinery, New York, NY, USA, 1–15.
- [75] Xuan Zhao, Mingming Fan, and Teng Han. 2022. “I Don’t Want People to Look At Me Differently”: Designing User-Defined Above-the-Neck Gestures for People with Upper Body Motor Impairments. In *Conference on Human Factors in Computing Systems - Proceedings*. Association for Computing Machinery.

A \$B Recognizer

A biosignal candidate gesture G or template T_i is composed of multiple *biosignals* b_j . Each *biosignal* may have one or more data *channels* c . Each channel is composed of a one-dimensional time-series *points* path (Fig. 1). The code is formatted according to Cormen et al. [15].

Step 1. For each biosignal channel c , resample the *points* path into n evenly spaced points using piecewise linear interpolation.

RESAMPLE(*points*, n)

input: *points* is an array of length N

n is the desired number of resampled time points

output: *newPoints* is an array of length n

```

1:  $N \leftarrow \text{LENGTH}(\textit{points})$ 
2:  $\textit{oldTime}, \textit{newTime} \leftarrow \text{TIME}(N, n)$ 
3:  $t_o \leftarrow 0$ 
4: initialize newPoints array
5: for time point  $t_n$  in newTime do
6:   while  $\textit{oldTime}_{t_o} < t_n$  do
7:      $t_o \leftarrow t_o + 1$ 
8:      $y_1, y_2 \leftarrow \textit{points}_{t_o-1}, \textit{points}_{t_o}$ 
9:      $x_1, x_2 \leftarrow \textit{oldTime}_{t_o-1}, \textit{oldTime}_{t_o}$ 
10:     $m \leftarrow \frac{y_2 - y_1}{x_2 - x_1}$  ▷ calculate slope
11:     $b \leftarrow y_2 - m \times x_2$  ▷ calculate intercept
12:     $q \leftarrow m \times t_n + b$  ▷ calculate new point
13:    APPEND(newPoints,  $q$ )
14: return newPoints

```

TIME(N, n)

input: N, n are integers corresponding to the array length of *points* and desired number of resampled time points

output: *oldTime*, *newTime* are arrays of length N and n , with the same initial and final time points 0 and N

```

1: index  $i \leftarrow 0$ 
2: initialize oldTime array
3: while index  $i < N$  do ▷ create array for old time
4:   APPEND(oldTime,  $i$ )
5:    $i \leftarrow i + 1$ 
6: index  $j \leftarrow 0$ 
7: initialize newTime array
8: while index  $j < n$  do ▷ create array for new time
9:   APPEND(newTime,  $\frac{j(N-1)}{n-1}$ )
10:   $j \leftarrow j + 1$ 
11: return oldTime, newTime

```

LENGTH(*points*)

input: *points* is an array of length N

output: N , the length of the input array

```

1:  $N \leftarrow 0$ 
2: for point  $p_i$  in points do
3:    $N \leftarrow N + 1$ 
4: return  $N$ 

```

Step 2. Scale *points* for channels c_i for a given biosignal b_j . DEMEAN sets each point p_i in *points* such that the mean of a channel c_i is equal to 0. STD takes the standard deviation of all channels for a given biosignal b_j . NORMALIZE scales the *points* such that the standard deviation of all channels c for a given biosignal b_j is equal to 1.

DEMEAN(*points*, n)

input: *points* are all points in a biosignal channel c_i
 n is the length of *points*

output: *newPoints* is an array with a mean of 0

- 1: **initialize** *newPoints* array
- 2: $\bar{p} \leftarrow \text{MEAN}(\text{points})$
- 3: **for** point p_i in *points* **do**
- 4: $q \leftarrow p_i - \bar{p}$
- 5: APPEND(*newPoints*, q)
- 6: **return** *newPoints*

NORMALIZE(*biosignal*)

input: *biosignal* is an array of all the channels c_i after the DEMEAN function is applied for a given biosignal b_j concatenated into one array

output: *newBiosignal* is an array of all the channels for a given biosignal with a standard deviation of 1

- 1: $\sigma \leftarrow \text{STD}(\text{biosignal})$
- 2: **initialize** *newPoints* array
- 3: **for** *points* in each *biosignal channel* **do**
- 4: **for** point p_i in *points* **do**
- 5: $q \leftarrow \frac{p_i}{\sigma}$
- 6: APPEND(*newPoint*, q)
- 7: APPEND(*newBiosignal*, *newPoints*)
- 8: **return** *newBiosignal*

MEAN(*points*, n)

input: *points* are all points in a biosignal channel c_i
 n is the length of *points*

output: \bar{p} is the average value of *points*

- 1: $\bar{p} \leftarrow 0$
- 2: **for** point p_i in *points* **do**
- 3: $\bar{p} \leftarrow \bar{p} + p_i$
- 4: $\bar{p} \leftarrow \frac{\bar{p}}{n}$
- 5: **return** \bar{p}

STD(*biosignal*)

input: *biosignal* is an array of all the channels c_i after the DEMEAN function is applied for a given biosignal b_j concatenated into one array

output: σ is the standard deviation of *biosignal*

- 1: $ix \leftarrow \text{LENGTH}(\text{biosignal})$
 - 2: $\bar{p} \leftarrow \text{MEAN}(\text{biosignal}, ix)$ \triangleright get mean of all signals
 - 3: $\sigma \leftarrow 0$
 - 4: **for** point p_i in *biosignal* **do**
 - 5: $\sigma \leftarrow \sigma + (p_i - \bar{p})^2$
 - 6: $\sigma \leftarrow \sqrt{\frac{1}{ix}\sigma}$
 - 7: **return** σ
-

Step 3. Compute template principal components and transformed points for nPC principal components. The input to the PCA is all points p across all channels c for all biosignals b concatenated into a matrix D with n timepoints and c biosignal channels (where c is the total number of channels for all measured biosignals). For these steps, we assume that all biosignal channels c are concatenated vertically such that the resulting data matrix D is comprised of c rows and n columns (i.e., D is a matrix of size $c \times n$). After this step, the *template* T_i points p are a concatenated one-dimensional signal. Note that while this step has multiple computations, there are many built-in algorithms (e.g., Python: `sklearn.decomposition.pca`; Java: `weka.attributeSelection.PrincipalComponents`; R: `stats.princomp`; Matlab: `pca`) that compute the PCs and transformed points. The built-in algorithms are often optimized such that the runtime is faster than implementing the PCA by hand [20].

PCA(D, c, n, nPC)

- 1: *covariance* \leftarrow COV(D, c, n) \triangleright Compute covariance matrix
- 2: *eigenvalues*, *eigenvectors* \leftarrow EIG(*covariance*) \triangleright Compute eigenvalues and eigenvectors
- 3: *sorted_eigenvectors* \leftarrow sort eigenvectors column-wise in order corresponding to the largest eigenvalue to the smallest in *eigenvalues*
- 4: $U \leftarrow$ the first nPC columns of *sorted_eigenvectors*
- 5: *points* \leftarrow MATMUL(D, U) \triangleright get transformed biosignal
- 6: *points* \leftarrow FLATTEN(*points*) \triangleright flatten transformed biosignal into a one-dimensional array
- 7: **return** principal components U , transformed one-dimensional *points*

COV(D, c, n)

input: D is a matrix of size c by n

output: *covariance* is a matrix of size c by c

- 1: **initialize** *covariance* matrix
- 2: **for** index $j = 1$ to c **do**
- 3: **initialize** *cov* array
- 4: **for** index $k = 1$ to c **do**
- 5: $sum \leftarrow 0$
- 6: **for** index $i = 1$ to n **do**
- 7: $sum \leftarrow sum + D_{j,i}D_{k,i}$
- 8: $sum \leftarrow \frac{sum}{n-1}$
- 9: APPEND(*cov*, sum)
- 10: APPEND(*covariance*, *cov*)

11: **return** *covariance*

EIG(*covariance*)

input: *covariance* is a matrix of size c by c

output: *eigenvalues* will be an array of length c , *eigenvectors* will be a matrix of size c by c

- 1: use a linear algebra package to compute eigenvalues and eigenvectors of covariance matrix
 - 2: **return** *eigenvalues*, *eigenvectors*
-

Step 3 cont.MATMUL(D, U)**input:** D^T is a matrix of size n by c U is a matrix of size c by nPC **output:** $newD$ is an array of length $nPC \times n$

- 1: $nPC \leftarrow$ column length of U
- 2: $n \leftarrow$ column length of D
- 3: **initialize** $newD$ matrix with nPC rows and n columns
(i.e., a matrix of size nPC by n)
- 4: **for** index $i = 1$ to n **do**
- 5: **for** index $j = 1$ to n **do**
- 6: **for** index $k = 1$ to nPC **do**
- 7: $newD_{i,j} \leftarrow D_{i,k}^T \times U_{k,j}$
- 8:
- 9: **return** $newPoints$

FLATTEN(D, nPC, n)**input:** D is a matrix of size nPC by n **output:** $newPoints$ is an array of length $nPC \times n$

- 1: **initialize** $newPoints$ array
- 2: $nPC, n \leftarrow$ row and column length of D
- 3: **for** index $i = 1$ to n **do**
- 4: **for** index $j = 1$ to n **do**
- 5: APPEND($newPoints, D_{i,j}$)
- 6: **return** $newPoints$

Step 4. Match candidate gesture G against each stored template T_i . G is resampled and normalized. The principal components U have already been computed for the templates and have already been transformed and flattened into a one-dimensional points array T_i . The candidate gesture G will be transformed and flattened into a one-dimensional points array during the template matching process.

RECOGNIZE(gesture $G, templates$)**input:** G is a matrix of size c by n

$templates$ are the set of templates T_i , each of which contains one-dimensional array of points p of length $nPC \times n$

output: matched template T'

score of final matched template

- 1: $b \leftarrow \infty$
- 2: **for each** template T_i in $templates$ **do**
- 3: $U \leftarrow$ principal components of T_i computed in Step 3
- 4: $points \leftarrow$ MATMUL(G^T, U)
- 5: $points \leftarrow$ FLATTEN($points$)
- 6: $d \leftarrow$ PATH – DISTANCE($points, T_i$)
- 7: **if** $d < b$ **then**
- 8: $b \leftarrow d$
- 9: $T' \leftarrow T_i$
- 10: **return** $\langle T' \rangle$

PATH-DISTANCE(A, B)**input:** A, B are both one-dimensional arrays**output:** distance d as a floating point

- 1: $d \leftarrow 0$
- 2: **for each** A_i, B_i in A, B **do**
- 3: $d \leftarrow d +$ DISTANCE(A_i, B_i)
- 4: **return** d

DISTANCE(A_i, B_i)**input:** A_i, B_i are both floating points**output:** distance d as a floating point

- 1: $d \leftarrow$ absolute value of $(A_i - B_i)$
- 2: **return** d

B Data Segmentation Pseudocode

We implemented a custom gesture segmentation method for our dataset based on the recorded raw EMG channels. We solely used the biosignal channels c from EMG data (16 EMG channels per gesture).

Data Segmentation. Our custom data segmentation method obtains different possible cutoff values based on heuristics and chooses the most conservative cutoff indices.

SEGMENT(G)

input: G is a matrix of size n time points by c channels of the absolute value of the raw EMG data

output: $start, stop$, segmentation cutoff indices

```

1:  $G_{rms} \leftarrow RMS(G)$ 
2:  $highest\_amplitude\_channels \leftarrow$  get 3 highest amplitude
3:   channels across all  $G$  for one participant
4:  $highest\_variance\_channels \leftarrow$  get 3 highest variance channels
5:   within one  $G$ 
6:  $relevant\_channels \leftarrow$  combine  $highest\_amplitude\_channels$ 
7:   and  $highest\_variance\_channels$ , remove duplicate channels
8:   and channels with variance below 0.1 of the maximum
9:   variance across channels
10: initialize  $allStart, allStop$  arrays
11: for each channel  $c$  in  $relevant\_channels$  do
12:    $Dc \leftarrow DIFF(c)$        $\triangleright$  take first difference across channel  $c$ 
13:    $D^2c \leftarrow DIFF(Dc)$    $\triangleright$  take second difference
14:   Compute different possible  $start, stop$  based on
15:     heuristics for  $c$ :
16:      $start_{Dc} \leftarrow LARGEST\_SLOPE(c, max = True)$ 
17:      $stop_{Dc} \leftarrow LARGEST\_SLOPE(c, max = False)$ 
18:      $start_{Below_1}, stop_{Below_1} \leftarrow THRESHOLD(c, value = 0.3)$ 
19:        $\triangleright$  Compute  $start, stop$  for aggressive threshold
20:      $start_{Below_2}, stop_{Below_2} \leftarrow THRESHOLD(c, value = 0.15)$ 
21:        $\triangleright$  Compute  $start, stop$  for conservative threshold
22:      $start_{Above_1}, stop_{Above_1} \leftarrow$ 
23:        $EDGE(c, THRESHOLD(c, value = 0.3))$ 
24:        $\triangleright$  Check if initial and final values in  $c$  surpass threshold
25:      $start_{Dc_1} \leftarrow LARGEST\_SLOPE(Dc, max = True)$ , restrict
26:        $Dc$  to indices between 0 and  $start_{Below_1}$ 
27:      $stop_{Dc_1} \leftarrow LARGEST\_SLOPE(Dc, max = False)$ , restrict
28:        $Dc$  to indices between  $stop_{Below_1}$  and end of array
29:      $start_{Dc_2} \leftarrow LARGEST\_SLOPE(Dc, max = True)$ , restrict
30:        $Dc$  to indices between 0 and  $start_{Below_1}$ 
31:      $stop_{Dc_2} \leftarrow LARGEST\_SLOPE(Dc, max = False)$ , restrict
32:        $Dc$  to indices between  $stop_{Below_2}$  and end of array
33:      $start_{D^2c_1} \leftarrow LARGEST\_SLOPE(D^2c, max = True)$ , restrict
34:        $D^2c$  to indices between 0 and  $start_{Below_1}$ 
35:      $stop_{D^2c_1} \leftarrow LARGEST\_SLOPE(D^2c, max = False)$ , restrict
36:        $D^2c$  to indices between  $stop_{Below_1}$  and end of array
37:     APPEND( $allStart$ , [ $start_{Dc}, start_{Above_1}, start_{Below_1},$ 
38:        $start_{Dc_1}, start_{Dc_2}, start_{D^2c_1}$ ])
39:     APPEND( $allStop$ , [ $stop_{Dc}, stop_{Above_1}, stop_{Below_1},$ 
40:        $stop_{Dc_1}, stop_{Dc_2}, stop_{D^2c_1}$ ])
41: Choose most conservative (i.e., the smallest index for
42:    $start$  and largest index for  $stop$ .)  $start, stop$  in
43:    $relevant\_channels$ :
44:    $start \leftarrow MIN(allStart)$ 
45:    $stop \leftarrow MAX(allStop)$ 
46: return  $start, stop$ 

```

Data Segmentation Cont.RMS(*points*, *window*, *overlap*)

input: *points* are all points in a biosignal channel c_i
window is the window size over which to compute the RMS over
overlap is the percent of overlap of each time window

output: *newPoints*, the root-mean-square of *points*

```

1: initialize newPoints array
2: for i in  $\frac{\text{LENGTH}(\text{points}) - \text{window}}{\text{overlap} \times \text{window}}$  do
3:   winPoints  $\leftarrow$  all points between
4:      $i \times \text{overlap} \times \text{window}$  to  $(i + 1) \times \text{window}$ 
5:   for point  $p_j$  in winPoints do
6:      $q \leftarrow \sqrt{\frac{1}{n} \sum_j p_j^2}$ 
7:     APPEND(newPoints, q)
8:   return newPoints

```

DIFF(*points*)

input: *points* are all points in a biosignal channel c_i

output: *newPoints*, the first discrete difference

```

1:  $N \leftarrow \text{LENGTH}(\text{points})$ 
2: initialize newPoints array
3: for index  $i = 1$  to  $N - 1$  do
4:    $q \leftarrow \text{points}_{i+1} - \text{points}_i$ 
5:   APPEND(newPoints, q)
6: return newPoints

```

ARGMAX,ARGMIN(*points*)

input: *points* are all points in a biosignal channel c_i

output: *argmax*, *argmin*, index of maximum or minimum value of *points*

```

1:  $i, \text{argmax}, \text{argmin} \leftarrow 0$ 
2:  $p_{\max} \leftarrow -\infty$ 
3:  $p_{\min} \leftarrow \infty$ 
4: for each point  $p$  in points do
5:   if  $p > p_{\max}$  then
6:      $p_{\max} = p$ 
7:      $\text{argmax} = i$ 
8:   if  $p < p_{\min}$  then
9:      $p_{\min} = p$ 
10:     $\text{argmin} = i$ 
11:    $i = i + 1$ 
12: return argmax or argmin

```

WHERE(*points logic value*)

gets all values in *points* that meet a *logic* criteria.

input: *points* are all points in a biosignal channel c
logic is the logical argument to compute Boolean over,
 e.g., $>$, $<$, $=$
value to compute logical argument over

output: *newPoints*, a Boolean array

```

1: for point in points do
2:   if  $\text{points}_i$  logic value then
3:     APPEND(newPoints, True)
4:   else
5:     APPEND(newPoints, False)
6: return newPoints

```

Heuristic *start*, *stop* Computations. Each computation is a different way to heuristically compute *start*, *stop* indices from our dataset. These heuristic methods were chosen based on extensive data exploration.

LARGEST_SLOPE(*points*, *max = True*)

input: *points* are all points in a biosignal channel c_i

output: *start*, *stop*, largest slope index for c

```

1: if max = True then
2:    $\text{start} \leftarrow \text{ARGMAX}(Dc)$   $\triangleright$  Get largest positive increase
3:   return start
4: else
5:    $\text{stop} \leftarrow \text{ARGMIN}(Dc) + 1$   $\triangleright$  Get largest negative increase
6:   return stop

```

EDGE(c , *thresh*)

input: *points* are all points in a biosignal channel c_i

thresh is the threshold**output:** *start*, *stop*, edge cases

```

1: initialize start  $\leftarrow$  NaN
2: if  $c_1 > \text{thresh}$  then
3:   start = 1
4: stop  $\leftarrow$  NaN
5: if  $c_N > \text{thresh}$  then  $\triangleright$  Where  $N = \text{LENGTH}(c)$ 
6:   stop = N

```

THRESHOLD(c , *value*)

input: c , a one-dimensional array

output: *start*, *stop* for a given threshold *value*

```

1:  $c_{\max} \leftarrow \text{MAX}(c)$   $\triangleright$  get maximum value in  $c$ 
2:  $c_{\min} \leftarrow \text{MIN}(c)$   $\triangleright$  get minimum value in  $c$ 
3:  $\text{threshold} \leftarrow \text{value}(c_{\max} - c_{\min}) + c_{\min}$ 
4:  $c_{\text{Below}} \leftarrow \text{WHERE}(c < \text{threshold})$ 
5:  $\triangleright$  Get all values in  $c$  below threshold
6: start  $\leftarrow$  first index of the output of WHERE(DIFF( $c_{\text{Below}}$ ) $>1$ )
7:  $\triangleright$  Return first instance where difference is below threshold
8: stop  $\leftarrow$  last index of the output of WHERE(DIFF( $c_{\text{Below}}$ ) $>1$ )
9:  $\triangleright$  Return last instance where difference is below threshold
10: return start, stop

```

Received 20 February 2007; revised 12 March 2009; accepted 5 June 2009